7,8-Dihydroxyflavone is a direct inhibitor of pyridoxal phosphatase

Christoph Zink[1,5], Linda Witzinger[1,5], Angelika Keller[1], Kerstin Hadamek[1], Sebastian Bothe[2], Martin Neuenschwander[3], Carmen Villmann[4], Jens Peter von Kries[3], Hermann Schindelin[2], Elisabeth Jeanclos[1,✉], Antje Gohla[1,✉]

[1] Institute of Pharmacology and Toxicology, University of Würzburg, Germany

[2] Rudolf Virchow Center for Integrative and Translational Bioimaging, University of Würzburg, Germany

[3] Leibniz-Forschungsinstitut für Molekulare Pharmakologie-FMP, Berlin, Germany

[4] Institute of Clinical Neurobiology, University Hospital, University of Würzburg, Germany

[5] Contributed equally

✉ Correspondence to: elisabeth.jeanclos@uni-wuerzburg.de or antje.gohla@uni-wuerzburg.de

ABSTRACT

Vitamin B6 deficiency has been linked to cognitive impairment in human brain disorders for decades. Still, the molecular mechanisms linking vitamin B6 to these pathologies remain poorly understood, and whether vitamin B6 supplementation improves cognition is unclear as well. Pyridoxal phosphatase (PDXP), an enzyme that controls levels of pyridoxal 5'-phosphate (PLP), the co-enzymatically active form of vitamin B6, may represent an alternative therapeutic entry point into vitamin B6-associated pathologies. However, pharmacological PDXP inhibitors to test this concept are lacking. We now identify a PDXP and age-dependent decline of PLP levels in the murine hippocampus that provides a rationale for the development of PDXP inhibitors. Using a combination of small molecule screening, protein crystallography and biolayer interferometry, we discover and analyze 7,8-dihydroxyflavone (7,8-DHF) as a direct and potent PDXP inhibitor. 7,8-DHF binds and reversibly inhibits PDXP with low micromolar affinity and sub-micromolar potency. In mouse hippocampal neurons, 7,8-DHF increases PLP in a PDXP-dependent manner. These findings validate PDXP as a druggable target. Of note, 7,8-DHF is a well-studied molecule in brain disorder models, although its mechanism of action is actively debated. Our discovery of 7,8-DHF as a PDXP inhibitor offers novel mechanistic insights into the controversy surrounding 7,8-DHF-mediated effects in the brain.

INTRODUCTION

Vitamin B6 is an essential micronutrient that plays an important role in the nervous system (1, 2), with the vitamin B6 status affecting cognitive function at any age (3, 4). Population studies indicate that low vitamin B6 levels are common among older people (5), and suggest that vitamin B6 deficiency may influence memory performance and may contribute to age-related cognitive decline (6-9). Vitamin B6 deficiency is also associated with other conditions characterized by impaired learning and memory, including neuropsychiatric disorders (10-12), Alzheimer's disease (13) and inflammation (14, 15). Nevertheless, the exact molecular mechanisms linking vitamin B6 to these pathologies are often insufficiently understood, and whether vitamin B6 supplementation improves cognition is unclear (4, 5, 16-22).

The term vitamin B6 encompasses the enzymatically interconvertible compounds pyridoxine, pyridoxamine, pyridoxal (referred to as B6 vitamers) and their phosphorylated forms. Among these, only pyridoxal 5′-phosphate (PLP) is co-enzymatically active. In humans, PLP is known to be required for 44 distinct biochemical reactions, including the biosynthesis and/or metabolism of neurotransmitters, amino acids, lipids, and glucose. In addition, B6 vitamers display antioxidant and anti-inflammatory functions (23-26).

Cellular PLP availability in the brain depends on numerous factors, including the intestinal absorption of B6 vitamers, extracellular phosphatases, inter-organ transport and intracellular enzymes and carriers/scavengers involved in PLP formation and homeostasis (2). Specifically, intracellular PLP is formed by the pyridoxal kinase (PDXK)-catalyzed phosphorylation of pyridoxal, or the pyridox(am)ine-5'-phosphate oxidase (PNPO)-catalyzed oxidation of pyridox(am)ine 5'-phosphate to PLP. PLP is highly reactive and can undergo condensation reactions with e.g., primary amino groups or thiol groups in proteins or amino

acids. Although the mechanisms of PLP delivery within the cells are still largely unknown, it is clear that the intracellular availability of PLP for co-enzymatic functions depends on PLP carriers/scavengers and on the hydrolytic activity of pyridoxal 5'-phosphate phosphatase (PDXP) (2, 27-30).

We have previously shown that the genetic knockout of PDXP (PDXP-KO) in mice increases brain PLP levels and improves spatial memory and learning, suggesting that elevated PLP levels can improve cognitive functions in this model (30). We therefore reasoned that a pharmacological inhibition of PDXP may be leveraged to increase intracellular PLP levels and conducted a high-throughput screening campaign to identify small-molecule PDXP modulators. Here, we report the discovery and the structural and cellular validation of 7,8-dihydroxyflavone (7,8-DHF) as a selective PDXP inhibitor. 7,8-DHF is a well-studied molecule in brain disorder models characterized by impaired cognition, and widely regarded as a tropomyosin receptor kinase B (TrkB) agonist with brain-derived neurotrophic factor (BDNF)-mimetic activity (31). However, a direct TrkB agonistic activity of 7,8-DHF has been called into question (32-36). Our serendipitous discovery of 7,8-DHF as a direct PDXP inhibitor provides an alternative mechanistic explanation for 7,8-DHF-mediated effects. More potent, efficacious, and selective PDXP inhibitors may be useful future tools to explore a possible benefit of elevated PLP levels in brain disorders.

RESULTS

PDXP activity controls PLP levels in the hippocampus

The hippocampus is important for age-dependent memory consolidation and learning, and impaired memory and learning is associated with PLP deficiency (3). To study a possible contribution of PDXP and/or PDXK to age-related PLP homeostasis in the hippocampus, we performed Western blot analyses in young versus older mice. Unexpectedly, we found that both PDXP and PDXK expression levels were markedly higher in hippocampi of middle-aged than of juvenile animals (**Fig. 1a**). These data suggest an accelerated hippocampal PLP turnover in older mice, consistent with previous findings in senescent mice (37).

An analysis of total hippocampal PLP levels in PDXP-WT and PDXP-KO mice showed an age-dependent profile. PLP levels appeared to peak around 3 months of age (possibly reflecting PLP-dependent neurotransmitter biosynthesis and metabolism during the postnatal developmental period) and descended back to juvenile levels by 12 months of age in both genotypes. Although total hippocampal PLP levels in PDXP-KO mice also decreased with age, they consistently remained above PLP levels in control mice (**Fig. 1b**; two-tailed, unpaired *t*-test of PLP levels in PDXP-WT vs. PDXP-KO hippocampi, all ages combined: $p<0.0001$).

PLP is protected from hydrolysis by binding to proteins, and PDXP is expected to dephosphorylate only non-protein-bound PLP (38). To test this, we prepared protein-depleted PLP fractions from PDXP-WT and PDXP-KO hippocampal lysates using 3 kDa molecular weight cutoff centrifugal filters. The quantification of PLP in these fractions demonstrated that PDXP loss indeed only increased the pool of protein-depleted PLP, both in young (18-42 days old) and older mice (252-352 days old, corresponding to mature/middle-aged mice), whereas the levels of protein-bound PLP remained unchanged (**Fig. 1c**). While the hippocampal levels of non-protein-bound PLP dropped by about 60% over this time span in PDXP-WT mice, they remained elevated in PDXP-KO mice ~2-fold higher in younger, and

116 ~5-fold higher in older PDXP-KO compared to the respective PDXP-WT; see **Fig. 1 – figure**
117 **supplement 1** for exact mouse ages). We conclude that hippocampi of older mice are
118 characterized by a specific decrease in the levels of non-protein-bound PLP, and that this age-
119 dependent PLP loss is dependent on PDXP activity. These observations establish that PDXP
120 is a critical determinant of PLP levels in the murine hippocampus and suggest that
121 intracellular PLP deficiency may be alleviated by PDXP inhibition.
122

123 **A high-throughput screening campaign identifies 7,8-dihydroxyflavone as a PDXP**
124 **inhibitor**

125 Pharmacological small-molecule PDXP inhibitors are currently lacking. To identify PDXP
126 inhibitor candidates, we screened the FMP small molecule repository containing 41,182
127 compounds for molecules able to modulate the phosphatase activity of recombinant, highly
128 purified murine PDXP (see **Fig. 2 – figure supplement 1** for a schematic of the screening
129 campaign). Difluoro-4-methylumbelliferyl phosphate (DiFMUP) was used as a fluorogenic
130 phosphatase substrate in a primary screen. Compounds that altered DiFMUP fluorescence by
131 ≥50% (activator candidates) or ≤25% (inhibitor candidates) were subjected to EC_{50}/IC_{50} value
132 determinations. Of these, 46 inhibitor hits were selected and counter-screened against
133 phosphoglycolate phosphatase (PGP), the closest PDXP relative (39, 40). Fourteen of the
134 PDXP inhibitor hits (with an IC_{50} PDXP <20 μM, and IC_{50} PDXP < IC_{50} PGP or no activity
135 against PGP) were subsequently validated in a secondary assay, using PLP as a physiological
136 PDXP substrate (see **Fig. 2 – figure supplement 2** for all 14 inhibitor hits). Only two PDXP-
137 selective inhibitor hits (FMP-1 and 7,8-dihydroxyflavone/7,8-DHF, a naturally occurring
138 flavone) blocked PDXP-catalyzed PLP dephosphorylation. FMP-1 (IC_{50} ~1 μM) was obtained
139 from an academic donor, and its structure is undisclosed for intellectual property reasons.
140 Further characterization was therefore only possible for 7,8-DHF (IC_{50} ~1 μM).

141 In vitro activity assays using PLP as a substrate confirmed that 7,8-DHF directly
142 blocks murine and human PDXP activity with submicromolar potency and an apparent
143 efficacy of ~50% (**Fig. 2a, b**). The efficacy of 7,8-DHF under these conditions may be limited
144 by the poor solubility of this flavone (see also **Fig. 2c**). This interpretation is supported by
145 Todd et al. who established a solubility profile of 7,8-DHF and demonstrated that only ~20%
146 of the compound remains in solution beyond a concentration of 5 μM (35).

147 We next examined whether commercially available 7,8-DHF analogs might be more
148 potent PDXP inhibitors. We tested flavone, 3,7-dihydroxyflavone, 5,7-dihydroxyflavone (also
149 known as chrysin), 3,5,7-trihydroxyflavon (galangin), 5,6,7-trihydroxyflavone (baicalein) and
150 3,7,8-trihydroxyflavone-4'-hydroxyphenyl. **Figure 2b** shows that of the tested 7,8-DHF
151 analogs, only 3,7,8-trihydroxyflavone-4'-hydroxyphenyl was able to inhibit PDXP, albeit
152 with an IC_{50} of 2.5 μM and thus slightly less potently than 7,8-DHF. These results suggest
153 that hydroxyl groups in positions 7 and 8 of the flavone scaffold are required for PDXP
154 inhibition.

155 We used a biolayer interferometry (BLI) optical biosensing technique to further
156 characterize the binding of 7,8-DHF to PDXP (**Fig. 2c**). Consistent with a specific interaction,
157 7,8-DHF binding to PDXP was concentration-dependent and fully reversible. Steady-state
158 analysis of a 7,8-DHF serial dilution series yielded an affinity (K_D) value of 3.1 ± 0.3 μM
159 (data are mean values ± S.E. of *n*=4 measurements; see **Fig. 2 – figure supplement 3** for the
160 three other measurements) using a 1:1 dose-response model. Global analysis of the
161 sensorgrams assuming a 1:1 binding model resulted in an affinity of 2.6 ± 0.5 μM, in line with
162 the steady-state results (**Fig. 2c**). Due to the aforementioned poor solubility of 7,8-DHF (35),
163 concentrations higher than 12.5 μM could not be evaluated. As expected, 5,7-
164 dihydroxyflavone showed no signal in the BLI, in line with previous experiments (see **Fig.**
165 **2b**). With its molecular size of 254 Da and its physicochemical properties, 7,8-DHF is a
166 typical fragment-like molecule (41). Typical association rate constants (k_{on}) for fragments are

167 limited by the rate of diffusion and are higher than 10^6 $M^{-1}s^{-1}$. Interestingly, 7,8-DHF showed
168 a slow k_{on} of 1050 $M^{-1}s^{-1}$, which is atypical and rarely found for fragment-like molecules
169 (42), and a k_{off} rate of 0.03 s^{-1}. With the commonly used estimation of $\Delta G \sim pK_D$ and a heavy
170 atom number of 19, 7,8-DHF shows a high ligand efficiency of 0.39, which makes it an
171 interesting molecule for further medicinal chemistry optimization. Taken together, these data
172 support a direct and reversible physical interaction between 7,8-DHF and PDXP that leads to
173 PDXP inhibition.
174
175 **Selectivity of 7,8-DHF**
176 PDXP is a member of the large family of haloacid dehalogenase (HAD)-type hydrolases (43).
177 HAD phosphatases are Mg^{2+}-dependent phospho-aspartate transferases that consist of a
178 Rossman-like catalytic core linked to a cap domain. The insertion site, structure and size of
179 the cap define the substrate selectivity of the respective enzyme. The "capless" C0-type HAD
180 phosphatases contain either a very small or no cap, resulting in an accessible catalytic cleft
181 that enables the dephosphorylation of macromolecular substrates. Larger C1 or C2 caps act as
182 a roof for the entrance to the active site; most C1/C2-capped HAD phosphatases consequently
183 dephosphorylate small molecules that can gain access to the catalytic cleft. Cap domains also
184 contain so-called substrate specificity loops that contribute to substrate coordination. Hence,
185 caps are distinguishing features of HAD phosphatases (38, 43-45).
186 To probe the selectivity of 7,8-DHF for PDXP, a C2-capped HAD phosphatase, we
187 tested five additional mammalian HAD phosphatases, including two other C2- and two C1-
188 capped phosphatases and one C0-type enzyme. When assayed at a (nominal) concentration of
189 5, 10 and 40 μM (i.e., up to ~40-fold above the IC_{50} value for PDXP-catalyzed PLP-
190 dephosphorylation), 7,8-DHF was inactive against four of the tested enzymes. 7,8-DHF
191 inhibited PGP, the closest PDXP relative, with an IC_{50} value of 4.8 μM (**Fig. 2d**). This result
192 is consistent with the criteria applied during the initial counter-screen (see above). Together,

193 our data show that 7,8-DHF selectively inhibits PDXP, and that higher 7,8-DHF
194 concentrations can also target the PDXP paralog PGP.
195
196 **Mode of PDXP inhibition**
197 To probe the mechanism of PDXP inhibition, we assayed the steady state kinetics of PLP
198 dephosphorylation in the presence of increasing 7,8-DHF concentrations (**Table 1**). Analysis
199 of the derived kinetic constants demonstrated that 7,8-DHF increased the K_M up to ~2-fold,
200 and slightly reduced v_{max} values ~0.7-fold. Thus, 7,8-DHF mainly exhibits a mixed mode of
201 PDXP inhibition, which is predominantly competitive.
202
203 **Co-crystal structure of PDXP bound to 7,8-DHF**
204 To investigate the mechanism of PDXP inhibition in more detail, we co-crystallized homo-
205 dimeric, full-length murine PDXP in complex with this compound. 7,8-DHF-bound PDXP
206 crystallized in the cubic space group I23 with one dimer per asymmetric unit, with protomer
207 A containing the inhibitor and protomer B representing an apo-state (**Fig. 3a**). The structure
208 was refined following molecular replacement with full-length murine PDXP (here referred to
209 as apo-PDXP; Protein Data Bank /PDB entry 4BX3) to a resolution of 2.0 Å resulting in an
210 R_{work} of 18.4% and an R_{free} of 21.1% (PDB code 8QFW). Data collection and refinement
211 statistics are summarized in **Table 2**.
212 Like apo-PDXP, 7,8-DHF-bound PDXP homodimerizes via its cap domain. The
213 alignment of the structures representing apo-PDXP, the inhibitor-free protomer B, and the
214 7,8-DHF-bound PDXP protomer A resulted in root mean square deviations (RMSDs) of 0.42
215 Å (A vs. B in this structure), 0.35 Å (A vs. B in 4BX3), 0.41 Å (A in this structure vs. A in
216 4BX3, **Fig. 3b**), 0.49 Å (A in this structure vs. B in 4BX3), 0.45 Å (B in this structure vs. A
217 in 4BX3) and 0.37 Å (B in this structure vs. B in 4BX3) based on Cα atoms, which indicate
218 that binding of the inhibitor did not result in significant changes in the backbone

219 conformations. In particular, we did not discern distinct open and closed active site
220 conformations (40) or a tilting of the substrate specificity loop (46) in 7,8-DHF-bound PDXP
221 compared to apo-PDXP. All catalytic core residues and the Mg^{2+} cofactor are correctly
222 oriented in the presence of the inhibitor. Hence, 7,8-DHF binding does not appear to impact
223 the overall fold or the open/closed dynamics of PDXP.

224 7,8-DHF was observed to only bind to one subunit (the A-chain; **Fig. 3a**) with well-
225 defined density (**Fig. 3c**) and full occupancy since its average B-factor of 45.8 $Å^2$ closely
226 matches the B-factors of the surrounding atoms. Binding to the other subunit (B-protomer) is
227 prevented by a salt bridge between Arg62 and Asp14 of a symmetry-related A-protomer (**Fig.**
228 **3d**). The χ_1 and χ_2 torsion angles of the Arg62 side chain observed in the B-protomer
229 correspond to those observed for this side chain in both protomers of the apo-structure
230 (4BX3). To allow binding of the inhibitor, the side chain of Arg62 needs to adopt a
231 completely extended conformation, which is prevented by the salt bridge.

232 It is currently unclear whether the PDXP crystal state with only a single inhibitor
233 bound per dimer reflects the state in solution. Due to the limited solubility of 7,8-DHF, we
234 were unable to address the stoichiometry of 7,8-DHF binding to the PDXP dimer with
235 isothermal calorimetry. It is conceivable that the PDXP crystal packing is very stable (indeed,
236 7,8-DHF-bound PDXP crystallized in the same cubic space group as apo-PDXP, see ref. (46),
237 including the aforementioned salt bridge between Arg62 of the B-subunit and Asp14 of a
238 symmetry-related molecule), and that the free energy generated by the formation of the crystal
239 lattice is higher than the free energy generated upon inhibitor binding. Further inspection of
240 7,8-DHF-bound PDXP indicated that the crystallographic neighbors of protomer A and B are
241 dissimilar. While the 7,8-DHF binding site is readily accessible in protomer A, the
242 corresponding site in protomer B is shielded by two crystallographic neighbors (**Fig. 3 –**
243 **figure supplement 1**).

244 In protomer A, 7,8-DHF binds directly in the PDXP active site, with its phenyl ring at
245 a distance of 8.3 Å from the Asp25 nucleophile, and 3.8 Å from Asp27, which functions as a
246 general acid/base in the two partial reactions of the catalytic cycle (47). The introduction of
247 PLP from PDB code 2CFT (human PDXP in complex with PLP) for visualization purposes
248 revealed a partial overlap between the PLP and 7,8-DHF binding sites (**Fig. 3e**). While PLP is
249 deeply buried in the catalytic cleft, the bulkier 7,8-DHF molecule obstructs the active site
250 entrance with its 1,4-benzopyrone moiety and its phenyl ring protrudes into the catalytic cleft.
251 7,8-DHF is embedded in a cavity of the PDXP active site that is exclusively formed by
252 the active site of protomer A, without a contribution of the dimerization interface with
253 protomer B. One side of this cavity is formed by the more polar residues Asp27, Asn60, Ser61
254 and Arg62, whereas the opposite side is established by the more hydrophobic residues
255 Tyr146, His178, Pro179, and Leu180. Adjacent to this hydrophobic stretch, the polar residue
256 Glu148 is located at the active site entrance, directly opposite of Arg62 on the more polar side
257 of the 7,8-DHF binding channel (**Fig. 3f**). Inhibitor binding appears to be primarily stabilized
258 by two hydrogen bonds, as well as polar and non-polar interactions. The side chain hydroxyl
259 group of Ser61 forms a direct hydrogen bond with the ketone group of the inhibitor, which is
260 additionally coordinated by the Ser61 backbone nitrogen atom. Furthermore, Glu148 forms a
261 direct hydrogen bond via its carboxylic acid with the 7-hydroxyl group of 7,8-DHF. The side
262 chains of the polar residues Asp27, Asn60, and Arg62 engage in van der Waals interactions
263 with 7,8-DHF. The two hydroxyl groups of the 7,8-DHF benzyl ring engage in van der Waals
264 interactions with the guanidinium group of Arg62 and the carboxylic acid function of Glu148.
265 On the more hydrophobic side of the binding cavity, Tyr146 forms π-electron stacking
266 interactions with the pyrone ring of 7,8-DHF. In addition, the His178 imidazole group
267 coordinates the 7,8-DHF phenyl ring via π-π stacking. His178, located in the substrate
268 specificity loop, and Asn60 and Arg62 are also important for PLP binding (46, 48). All PDXP

269 residues found to engage in 7,8-DHF interactions are identical in murine and human PDXP
270 (**Fig. 3 – figure supplement 2**).

271 To verify the putative 7,8-DHF – PDXP interactions, we introduced single mutations
272 into the binding interface. Asn60, Arg62, Tyr146, Glu148 and His178 were each exchanged
273 for Ala ($PDXP^{N60A}$, $PDXP^{R62A}$, $PDXP^{Y146A}$, $PDXP^{E148A}$, or $PDXP^{H178A}$, respectively). Since
274 the carboxamide group of Asn60 can form a hydrogen bond with the carboxylate moiety of
275 the Asp27, and a loss of this interaction in the $PDXP^{N60A}$ variant is predicted to alter the
276 PDXP structure, we additionally mutated Asn60 to Ser ($PDXP^{N60S}$). PDXP variants were
277 recombinantly expressed and purified from *E. coli* (see **Fig. 3 – figure supplement 3** for
278 protein purity). **Figure 3g** (left panel) shows that all PDXP variants were enzymatically
279 active. As expected, the phosphatase activities of $PDXP^{N60A}$ and of $PDXP^{H178A}$ were reduced.
280 The somewhat elevated phosphatase activity of $PDXP^{Y146A}$ and $PDXP^{E148A}$ is currently
281 unexplained. Importantly, all variants except $PDXP^{N60A}$ and $PDXP^{N60S}$ were resistant to 7,8-
282 DHF, supporting the essential role of each of these residues for inhibitor binding (**Fig. 3g**,
283 right panel).

284 Based on the inhibitor-bound structure and the predominantly competitive component
285 of PDXP inhibition by 7,8-DHF (increased K_M, see **Table 1**), it seems likely that 7,8-DHF
286 sterically hinders substrate access to the active site, and competes with PLP coordination. In
287 addition, BLI measurements (see **Fig. 2c**) showed a relatively slow association rate and
288 extended residence time of 7,8-DHF (τ=30.3 s). This may indicate a possible reorganization
289 of the amino acids and water molecules within the binding site as a function of slow-onset
290 7,8-DHF binding. The reduced rate of product formation may account for the observed non-
291 competitive component of 7,8-DHF-mediated PDXP inhibition (reduction of v_{max}, see **Table**
292 **1**).

293

294 **7,8-DHF functions as a PDXP inhibitor in hippocampal neurons**

295 To investigate cellular target engagement of 7,8-DHF, we isolated primary hippocampal
296 neurons from PDXP-WT and PDXP-KO embryos. PDXP deficiency increased total PLP
297 levels 2.4-fold compared to PDXP-WT neurons (**Fig. 4a**). This finding is in good agreement
298 with the PLP increase resulting from PDXP loss in total hippocampal extracts (see **Fig. 1**).
299 The larger absolute PLP values in cultured neurons are likely attributable to the high
300 concentration of the PLP precursor pyridoxal (20 μM) in the culture medium. We did not
301 observe PDXP-dependent changes in pyridoxal kinase (PDXK) expression (**Fig. 4b**) and
302 could not detect pyridox(am)ine-5'-phosphate oxidase (PNPO) in hippocampal neuronal
303 cultures, suggesting that the PLP increase was primarily caused by the constitutive PDXP
304 loss.

305 To assess the consequences of 7,8-DHF treatment on PLP levels in hippocampal
306 neurons, we chose short-term incubation conditions (45 min, 20 μM) to avoid possible
307 secondary effects of the inhibitor. As expected, the acute effect of 7,8-DHF treatment in WT
308 cells was much more subtle (~9% increase in total PLP) than the impact of long-term PDXP-
309 deficiency (441.3 ± 62.6 nmol PLP/g protein in DMSO solvent control-treated cells versus
310 482.7 ± 130.4 nmol PLP/g protein in 7,8-DHF treated cells; data are mean values ± S.E. of
311 *n*=4 independent experiments). However, this effect is likely underestimated because only the
312 PDXP-accessible pool of non-protein-bound PLP may be impacted by 7,8-DHF (see **Fig. 1c**).
313 Due to the limited number of available hippocampal neurons, we were unfortunately unable to
314 obtain sufficient quantities of protein-depleted PLP pools to address this question.

315 Acute changes in the PLP/PL ratio may be a more sensitive indicator of PDXP activity
316 than changes in total PLP levels alone, because PDXP inhibition is expected to increase
317 cellular levels of PLP (the PDXP substrate) and to concomitantly decrease the levels of PL
318 (the product of PDXP phosphatase activity). The PLP/PL ratio is also independent of the
319 exact protein concentration in a given extract of hippocampal neurons, thus optimizing
320 comparability between samples. As shown in **Fig. 4c**, 7,8-DHF significantly increased the

321 PLP/PL ratio in PDXP-WT, but not in PDXP-KO hippocampal neurons (+18% versus +1%
322 compared to the respective DMSO controls). Together, these data indicate that 7,8-DHF can
323 modulate cellular PLP levels in a PDXP-dependent manner and validate PDXP as a 7,8-DHF
324 target in primary hippocampal neurons.
325
326

327 **DISCUSSION**

328

329 PLP deficiency has been associated with human brain disorders for decades (3), yet causal
330 links remain unclear. Aside from vitamin B6 administration, pharmacological strategies to
331 elevate intracellular PLP levels are lacking. Here, we identify 7,8-dihydroxyflavone (7,8-
332 DHF) as a direct PDXP inhibitor that increases PLP levels in hippocampal neurons, validating
333 PDXP as a druggable target to control intracellular PLP levels in the brain. We also present a
334 high-resolution 7,8-DHF/PDXP co-crystal structure that could facilitate the design of more
335 potent, efficacious, and selective PDXP inhibitors in the future. Such molecules might
336 improve the control of intracellular PLP levels and help to elucidate a possible contribution of
337 PLP to the pathophysiology of brain disorders. Our observation that the expression of PDXP
338 is substantially upregulated in hippocampi of middle-aged mice suggests that a therapeutic
339 vitamin B6 supplementation alone may not suffice to elevate intracellular PLP levels under
340 conditions where the PLP-degrading phosphatase is hyperactive.

341 The discovery of 7,8-DHF as a direct PDXP inhibitor was unexpected. Interestingly,
342 numerous in vivo studies have reported the effectiveness of 7,8-DHF in brain disorder
343 models, including rodent models of Alzheimer's disease (49-56), depression (57-62),
344 schizophrenia (63-67), or epilepsy (68, 69), as well as in rodent models of autism (70-73).
345 Although PLP deficiency is thought to contribute to the respective human conditions (3, 74,
346 75), PLP-dependent processes have not yet been considered in the context of 7,8-DHF-
347 induced effects.

348 7,8-DHF was initially discovered as a small-molecule TrkB agonist with BDNF-
349 mimetic activity (76). BDNF, a high-affinity TrkB ligand, is an important neuropeptide for
350 nervous system function and pathology. Consensus is emerging that BDNF plays a key role in
351 the treatment response to neuropsychiatric drugs (32). Therapeutics that target BDNF/TrkB-
352 signaling are thus of interest as disease-modifying agents in several brain disorders. Since

353 BDNF does not cross the blood-brain barrier, attempts have been made to develop small
354 molecule BDNF mimetics. Several candidates have been reported, including 7,8-DHF (33,
355 76). Nevertheless, the on-target selectivity and efficacy of these compounds is actively
356 debated. Using quantitative and direct assays to measure TrkB dimerization and activation,
357 TrkB downstream signaling pathways, TrkB-dependent gene expression and cytoprotection,
358 7,8-DHF and other reported small-molecule TrkB agonists failed to activate TrkB in cells (33-
359 35). An electrophysiological study in acute hippocampal slice preparations demonstrated that
360 7,8-DHF potentiates hippocampal mossy fiber-CA3 synaptic transmission in a TrkB receptor-
361 independent manner (77). Overall, it appears that the mechanism of action of 7,8-DHF is
362 incompletely understood, but 7,8-DHF targets other than TrkB so far have remained elusive.
363 The identification of 7,8-DHF as a PDXP inhibitor reported here indicates that this flavone
364 may modulate vitamin B6-dependent processes and suggests that PDXP could be explored as
365 a pharmacological entry point into brain disorders.
366
367

MATERIALS AND METHODS

Materials

Unless otherwise specified, all reagents were of the highest available purity and purchased from Sigma-Aldrich (Schnelldorf, Germany). 3,7,8-Trihydroxyflavone-4‘-hydroxyphenyl was obtained from Ambinter (Orléans, France), all other flavones were from Sigma-Aldrich.

PDXP knockout mice

Floxed PDXP mice (*Pdxp*^{tm1Goh}) were generated on a C57Bl/6J background, and whole-body *Pdxp* knockouts were achieved by breeding with B6.FVB-Tg(EIIa-cre)C5379Lmgd/J (EIIa-Cre) transgenic mice, as described (30). All experiments were authorized by the local veterinary authority and committee on the ethics of animal experiments (Regierung von Unterfranken). All analyses were carried out in strict accordance with all German and European Union applicable laws and regulations concerning care and use of laboratory animals.

Preparation of hippocampi and hippocampal neurons and immunocytochemistry

Mice were sacrificed by cervical dislocation, and brains were immediately placed on a pre-cooled metal plate and dissected under a Leica M80 binocular (Leica, Wetzlar, Germany). Hippocampi were weighed and flash-frozen in liquid nitrogen. The entire procedure was performed in <3 min. Hippocampal lysates were prepared by the addition of ice-cold PBS (200 µL PBS/10 mg hippocampal wet weight) and homogenized for 1 min in a TissueLyser II instrument (Qiagen, Hilden, Germany). One fourth of the obtained volume of each lysate was used for the analysis of total PLP concentrations as described below. To determine protein-depleted PLP (27), the remaining volume of each lysate was centrifuged at 14,000 × *g* for 15 min at 4°C. The supernatant was applied to 3 kDa MWCO filters (Amicon Ultra-0.5

394 Centrifugal Filter; Merck Millipore, Darmstadt, Germany), and centrifuged at 14,000 × g for
395 45 min at 4°C. The flow-through was collected and prepared for HPLC analysis (see below).
396 Primary hippocampal neuronal cultures were prepared from mouse embryos at
397 embryonic day 17. Hippocampi were incubated with 0.5 mg/mL trypsin, 0.2 mg/mL EDTA
398 and 10 µg/mL DNase I in PBS for 30 min at 37°C. Trypsinization was stopped by adding
399 10% fetal calf serum. Cells were dissociated by trituration, counted, and seeded at a density of
400 150,000 cells per 35 mm dish. Dissociated cells were grown in neurobasal medium
401 supplemented with L-glutamine and B27 supplement (A3582801, Life Technologies,
402 Dreieich, Germany) with an exchange of 50% of the medium after 6 days in culture. After 21
403 days of differentiation (day in vitro 21/DIV21), 7,8-DHF (20 µM) or DMSO (0.02%, v/v) was
404 added to the hippocampal neuronal cultures for 45 min. Cells were rinsed once with PBS
405 (37°C), lysed in 150 µL ice cold H_2O, and placed at -80°C for at least 30 min.
406 For immunocytochemistry, DIV21 primary hippocampal neurons were fixed with 4%
407 (w/v) paraformaldehyde in phosphate-buffered saline (PBS) for 15 min at RT. After washing
408 twice with PBS, 50 mM NH_4Cl was added for 10 min. Cells were then permeabilized with
409 0.1% (v/v) Triton X-100 and blocked with 5% (v/v) goat serum in PBS for 30 min at 22°C.
410 Cells were incubated with mouse monoclonal anti-MAP2 antibodies (1:500 dilution, clone
411 MAB3418, Millipore, Darmstadt, Germany) for 1 h in 5% goat serum/PBS at 22°C. Alexa-
412 488-labeled secondary goat anti-mouse antibodies (1:500 dilution; Dianova, Hamburg,
413 Germany) were applied for 1 h. Nuclei were counter-stained with 4',6-diamino-2-
414 phenylindole (DAPI), and slides were mounted with Mowiol. Images were acquired using an
415 inverted IX81 microscope equipped with an Olympus UPLSAPO 60× oil objective
416 (numerical aperture: 1.35) on an Olympus FV1000 confocal laser scanning system, using a
417 FVD10 SPD spectral detector and diode lasers of 405 nm (DAPI) and 495 nm (Alexa488).
418
419 **Determination of PLP and PL by high-performance liquid chromatography (HPLC)**

420 Samples were derivatized as described (78). Briefly, 100 µL of lysate were mixed with 8 µL
421 derivatization agent (containing 250 mg/mL of both semicarbazide and glycine), and
422 incubated on ice for 30 min. Samples were then deproteinized by addition of perchloric acid
423 (8 µL of a 72% (w/v) stock solution), followed by centrifugation at 15,000 × *g* for 15 min at 4
424 °C. Supernatants (100 µL) were neutralized with 10 µL NaOH (25% (v/v) stock solution), and
425 2 µM pyridoxic acid was added as an internal standard. PLP and PL were subjected to the
426 same derivatization protocol to establish a standard curve. Samples were analyzed on a
427 Dionex Ultimate 3000 HPLC (Thermo Fisher Scientific, Dreieich, Germany), using 60 mM
428 Na_2HPO_4, 1 mM EDTA, 9.5% (v/v) MeOH; pH 6.5 as mobile phase. PL, PLP and pyridoxic
429 acid were separated on a 3 µm reverse phase column (BDS-HYPERSIL-C18, Thermo Fisher
430 Scientific). Chromatograms were analyzed using Chromeleon 7 software (Thermo Fisher
431 Scientific).
432
433 **Western blotting**
434 Tissue or cell homogenates (prepared as detailed above for HPLC analysis) were extracted
435 with 4 × RIPA buffer (final concentration, 50 mM Tris, pH 7.5; 150 mM NaCl, 1% (v/v)
436 Triton X-100, 0.5% (v/v) sodium deoxycholate, 0.1% (w/v) SDS, 1 mM 4-(2-
437 aminoethyl)benzenesulfonyl fluoride (Pefabloc), 5 µg/mL aprotinin, 1 µg/mL leupeptin, 1
438 µg/mL pepstatin) for 15 min at 4 °C under rotation, and lysates were clarified by
439 centrifugation (20,000 × *g*, 15 min, 4 °C). Protein concentrations in the supernatants were
440 determined using the Micro BCA Protein Assay Kit (Thermo Fisher Scientific). Proteins were
441 separated by SDS-PAGE and transferred to nitrocellulose membranes by semidry-blotting.
442 Antibodies were purchased from the following providers: Merck Millipore (mouse
443 monoclonal α-actin mAb1501, dilution 1:5000); Cell Signaling (rabbit monoclonal α-PDXP
444 clone C85E3, dilution 1:1000; Cell Signaling, Danvers/Massachusetts, USA), Sigma
445 Aldrich (rabbit polyclonal α-PDXK/AB1, #AV53615, dilution 1:1000), and Thermo Fisher

Scientific (rabbit polyclonal α-PNPO, #PA5-26400, dilution 1:1000, as used in ref. (30)). Western blots were densitometrically quantified with NIH ImageJ, version 1.45i.

Phosphatase plasmids and cloning

N-terminally GST-tagged, human PDXP was in pGEX-4T-1 (Amersham Biosciences, Amersham, UK). All other phosphatases were of murine origin and were subcloned into pETM11 (EMBL), as described (40). *Pdxp* point mutants (generated by nested PCR) were subcloned into the *Nco*I (*Pci*I for *Psph*) and *EcoR*I restriction sites of pETM11, using Q5 Hot Start High-Fidelity DNA Polymerase (New England Biolabs, Frankfurt/Main, Germany). The following primers (oligonucleotide sequence 5´- 3´; fwd, forward; rev, reverse) were used:

Pdxp	fwd: TCGACCATGGCGCGCTGCGAGCGG
	rev: AAAAGTGAATTCTCAGTCCTCCAGCCCCTC
Pdxp-N60A	fwd: TTCGTGAGCAACGCCAGCCGGCGCGCG
	rev: CGCGCGCCGGCTGGCGTTGCTCACGAA
Pdxp-N60S	fwd: TTCGTGAGCAACAGCAGCCGGCGCGCG
	rev: CGCGCGCCGGCTGCTGTTGCTCACGAA
Pdxp-R62A	fwd: AGCAACAACAGCGCGCGCGCGCGGCCC
	rev: GGGCCGCGCGCGCGCGCTGTTGTTGCT
Pdxp-Y146A	fwd: GTGCTCGTAGGCGCCGACGAGCAGTTT
	rev: AAACTGCTCGTCGGCGCCTACGAGCAC
Pdxp-E148A	fwd: GTAGGCTACGACGCGCAGTTTTCCTTC
	rev: GAAGGAAAACTGCGCGTCGTAGCCTAC
Pdxp-H178A	fwd: CGCGACCCTTGGGCCCCGCTCAGCGAC
	rev: GTCGCTGAGCGGGGCCCAAGGGTCGCG

Primers were purchased from Eurofins Genomics (Ebersberg, Germany), and all constructs were verified by sequencing (Microsynth Seqlab, Göttingen, Germany).

472 **Expression and purification of recombinant proteins**

473 All purification steps of murine PDXP and murine PGP were carried out exactly as described
474 (40). N-terminally His_6-tagged PDXP variants were expressed exactly as described for PDXP-
475 WT (40), except that the His_6-tag was not cleaved off. Human GST-PDXP was transformed
476 into *E. coli* BL21(DE3) (Stratagene Europe/VWR, Darmstadt, Germany). Protein expression
477 was induced with 0.5 mM isopropyl β-d-thiogalactopyranoside for 18 h at 20 °C. All
478 subsequent purification steps were carried out at 4 °C. Cells were harvested by centrifugation
479 for 10 min at 8000 × *g* and resuspended in lysis buffer (100 mM triethanolamine/TEA,
480 500 mM NaCl; pH 7.4) supplemented with protease inhibitors (EDTA-free protease inhibitor
481 tablets; Roche, Mannheim, Germany) and 150 U/mL DNase I (Applichem, Renningen,
482 Germany). Cells were lysed using a cell disruptor (Constant Systems, Daventry, UK), and cell
483 debris was removed by centrifugation for 30 min at 30,000 × *g*. GST-PDXP was batch-
484 purified on a glutathione sepharose 4B resin (GE Healthcare, Uppsala, Sweden). After
485 extensive washing with 25 column volumes of wash buffer (50 mM TEA, 250 mM NaCl; pH
486 7.4), GST-PDXP was eluted in wash buffer supplemented with 10 mM reduced glutathione,
487 concentrated, and further purified in buffer A (50 mM TEA, 250 mM NaCl, 5 mM $MgCl_2$; pH
488 7.4). using a HiLoad 16/60 Superdex 200 pg gel filtration column operated on an ÄKTA
489 liquid chromatography system (GE Healthcare).

490

491 **High-Throughput Screen for PDXP Modulators**

492 The screening campaign (chemical library, screening protocol, concentration-dependent
493 assays, data analysis) was conducted exactly as described previously (40), except that the
494 primary screen was done with PDXP, the counter-screen was done with PGP, and PDXP
495 inhibitor hits were validated using 5'-pyridoxal phosphate (PLP) as a physiological PDXP
496 substrate.

497

498 **IC_{50} determinations, enzyme kinetics, and compound selectivity**

499 Buffer conditions for enzymatic assays were as previously published (40). Purified
500 phosphatases were pre-incubated for 10 min at RT with serial dilutions of flavones.
501 Dephosphorylation reactions were started by the addition of the indicated substrate; buffer
502 with substrate and the respective flavone but without the enzyme served as a background
503 control. Prior to compound testing, time courses of inorganic phosphate release from the
504 respective phosphatase substrates were conducted to ensure assay linearity. Inorganic
505 phosphate release was detected with malachite green solution (Biomol Green; Enzo Life
506 Sciences, Lörrach, Germany); the absorbance at 620 nm (A_{620}) was measured on an Envision
507 2104 multilabel reader (Perkin Elmer, Rodgau, Germany). Released phosphate was
508 determined by converting the values to nmol P_i with a phosphate standard curve. Data were
509 analyzed with GraphPad Prism version 9.5.1 (GraphPad, Boston/Massachusetts, USA). For
510 IC_{50} determinations, $\log_{inhibitor}$ versus response was calculated (four parameter). To derive K_M
511 and k_{cat} values, data were fitted by nonlinear regression to the Michaelis-Menten equation.

512

513 **Biolayer interferometry (BLI)**

514 PDXP was biotinylated using the EZ-Link NHS-PEG4-Biotin kit, as recommended by the
515 manufacturer (Thermo Fisher Scientific), and loaded on Super Streptavidin Biosensors (SSA)
516 (Sartorius, Göttingen, Germany) as follows. SSA sensors were equilibrated for 1 h at RT in
517 BLI assay buffer (250 mM triethanolamine, 5 mM $MgCl_2$, 250 mM NaCl, 0.005% (v/v)
518 TWEEN-20; pH 7.5), loaded with 200 µg/mL biotinylated PDXP, blocked with 2 µg/mL
519 biocytin, and washed in BLI assay buffer. Reference SSA sensors were blocked with 2 µg/mL
520 biocytin (79). Six point 1:1 serial dilution series of 7,8-DHF and 5,7-DHF were prepared in
521 DMSO, and BLI assay buffer was added to the wells to obtain a 7,8-DHF starting
522 concentration of 25 µM. The final DMSO concentration was 5% (v/v). Buffers for baseline,
523 dissociation, and buffer correction wells were supplemented with the same amount of DMSO

524 for identical buffer conditions. Four measurements were carried out per condition, using one
525 sensor set for two measurements. All measurements were conducted on an Octet K2 device
526 (Sartorius) using 96-well plates. Assay settings were as follows: baseline measurement 45 sec,
527 association time 90 sec, dissociation time 150 sec. The resulting data were processed using
528 the double reference method of the Octet analysis software for removal of drifts and well-to-
529 well artefacts. Kinetic analyses were performed using the Octet analysis software. The steady
530 state analysis was carried out with OriginPro 2021b (OriginLab, Northampton/Massachusetts,
531 USA), using a dose-response model for regression.
532
533 **PDXP crystallization and data collection**
534 For co-crystallization with 7,8-DHF, full-length murine PDXP (10 mg/mL in 50 mM
535 triethanolamine; 250 mM NaCl; 5 mM $MgCl_2$; pH 7.4) was supplemented with a three-fold
536 molar excess of the flavone. Prism-shaped crystals of 7,8-DHF-bound PDXP were grown at
537 20°C in 0.1 M phosphate citrate (pH 4.2) and 40% (v/v) PEG 300 using the sitting-drop vapor
538 diffusion method. Crystals were cryoprotected for flash-cooling in liquid nitrogen by soaking
539 in mother liquor 25% (v/v) glycerol. Diffraction data were collected from flash-cooled
540 crystals after addition of 25% glycerol at a temperature of 100 K on beamline BL 14.1 at the
541 BESSY (Helmholtz Zentrum Berlin, Germany) synchrotron. The structure of 7,8-DHF-PDXP
542 was solved by molecular replacement with the program Phaser (80) with the structure of the
543 murine PDXP (PDB entry 4BX3) as search model.
544

ACKNOWLEDGMENTS

We thank Carola Seyffarth and Nicole Bader for excellent technical assistance, Dr. Jochen Kuper for collecting the diffraction data and the staff at beamline BL14.1 of the BESSY synchrotron.

DATA AVAILABILITY STATEMENT

The previously published PDB entry 4BX3 [http://doi.org/10.2210/pdb4BX3/pdb] of murine apo-PDXP and 2CFT [http://doi.org/10.2210/pdb2CFT/pdb] of PLP-bound human PDXP are used in this manuscript. X-ray crystallographic data of 7,8-DHF-bound PDXP generated in this study have been deposited in the PDB and can be accessed under the PDB entry 8QFW [http://doi.org/10.2210/pdb8QFW/pdb].

AUTHOR CONTRIBUTIONS

Conceptualization, A.G.; validation, E.J.; formal analysis, C.Z., L.W., S.B., M.N., H.S., E.J., A.G.; investigation, C.Z., L.W., A.K., K.H., S.B., M.N., E.J.; resources, C.V., M.N., J.P.v.K., H.S.; writing – original draft preparation, A.G. with input from E.J. and H.S.; visualization, C.Z., L.W., S.B., E.J., A.G.; supervision, E.J., A.G.; project administration, A.G.; funding acquisition, A.G.

COMPETING INTERESTS

The authors declare no competing interests.

567 **REFERENCES**

568 1. F. G. Bowling, Pyridoxine supply in human development. *Semin Cell Dev Biol* **22**, 611-618
569 (2011).
570 2. M. P. Wilson, B. Plecko, P. B. Mills, P. T. Clayton, Disorders affecting vitamin B(6) metabolism.
571 *J Inherit Metab Dis* **42**, 629-646 (2019).
572 3. M. L. di Salvo, M. K. Safo, R. Contestabile, Biomedical aspects of pyridoxal 5'-phosphate
573 availability. *Front Biosci (Elite Ed)* **4**, 897-913 (2012).
574 4. E. S. Mitchell, N. Conus, J. Kaput, B vitamin polymorphisms and behavior: evidence of
575 associations with neurodevelopment, depression, schizophrenia, bipolar disorder and
576 cognitive decline. *Neurosci Biobehav Rev* **47**, 307-320 (2014).
577 5. R. Malouf, J. Grimley Evans, The effect of vitamin B6 on cognition. *Cochrane Database Syst*
578 *Rev* 10.1002/14651858.CD004393, CD004393 (2003).
579 6. C. F. Hughes *et al.*, B-Vitamin Intake and Biomarker Status in Relation to Cognitive Decline in
580 Healthy Older Adults in a 4-Year Follow-Up Study. *Nutrients* **9** (2017).
581 7. K. Jannusch *et al.*, A Complex Interplay of Vitamin B1 and B6 Metabolism with Cognition,
582 Brain Structure, and Functional Connectivity in Older Adults. *Front Neurosci* **11**, 596 (2017).
583 8. H. Xu, S. Wang, F. Gao, C. Li, Vitamin B(6), B(9), and B(12) Intakes and Cognitive Performance
584 in Elders: National Health and Nutrition Examination Survey, 2011-2014. *Neuropsychiatr Dis*
585 *Treat* **18**, 537-553 (2022).
586 9. M. F. Elias *et al.*, Homocysteine, folate, and vitamins B6 and B12 blood levels in relation to
587 cognitive performance: the Maine-Syracuse study. *Psychosom Med* **68**, 547-554 (2006).
588 10. Y. Tomioka *et al.*, Decreased serum pyridoxal levels in schizophrenia: meta-analysis and
589 Mendelian randomization analysis. *J Psychiatry Neurosci* **43**, 194-200 (2018).
590 11. K. Toriumi *et al.*, Vitamin B6 deficiency hyperactivates the noradrenergic system, leading to
591 social deficits and cognitive impairment. *Transl Psychiatry* **11**, 262 (2021).
592 12. M. Arai *et al.*, Enhanced carbonyl stress in a subpopulation of schizophrenia. *Arch Gen*
593 *Psychiatry* **67**, 589-597 (2010).
594 13. B. D. Paul, Neuroprotective Roles of the Reverse Transsulfuration Pathway in Alzheimer's
595 Disease. *Front Aging Neurosci* **13**, 659402 (2021).
596 14. P. M. Ueland, A. McCann, O. Midttun, A. Ulvik, Inflammation, vitamin B6 and related
597 pathways. *Mol Aspects Med* **53**, 10-27 (2017).
598 15. L. G. Danielski *et al.*, Vitamin B(6) Reduces Neurochemical and Long-Term Cognitive
599 Alterations After Polymicrobial Sepsis: Involvement of the Kynurenine Pathway Modulation.
600 *Mol Neurobiol* **55**, 5255-5268 (2018).
601 16. Z. Wang, W. Zhu, Y. Xing, J. Jia, Y. Tang, B vitamins and prevention of cognitive decline and
602 incident dementia: a systematic review and meta-analysis. *Nutr Rev* **80**, 931-949 (2022).
603 17. A. Behrens, E. Graessel, A. Pendergrass, C. Donath, Vitamin B-Can it prevent cognitive
604 decline? A systematic review and meta-analysis. *Syst Rev* **9**, 111 (2020).
605 18. B. Hassel, A. G. Rogne, S. Hope, Intellectual Disability Associated With Pyridoxine-Responsive
606 Epilepsies: The Need to Protect Cognitive Development. *Front Psychiatry* **10**, 116 (2019).
607 19. A. W. Rutjes *et al.*, Vitamin and mineral supplementation for maintaining cognitive function
608 in cognitively healthy people in mid and late life. *Cochrane Database Syst Rev* **12**, CD011906
609 (2018).
610 20. A. D. Smith, H. Refsum, Homocysteine, B Vitamins, and Cognitive Impairment. *Annu Rev Nutr*
611 **36**, 211-239 (2016).
612 21. P. S. Aisen *et al.*, High-dose B vitamin supplementation and cognitive decline in Alzheimer
613 disease: a randomized controlled trial. *JAMA* **300**, 1774-1783 (2008).
614 22. G. Douaud *et al.*, Preventing Alzheimer's disease-related gray matter atrophy by B-vitamin
615 treatment. *Proc Natl Acad Sci U S A* **110**, 9523-9528 (2013).
616 23. R. Percudani, A. Peracchi, A genomic overview of pyridoxal-phosphate-dependent enzymes.
617 *EMBO Rep* **4**, 850-854 (2003).

618 24. A. C. Eliot, J. F. Kirsch, Pyridoxal phosphate enzymes: mechanistic, structural, and
619 evolutionary considerations. *Annu Rev Biochem* **73**, 383-415 (2004).
620 25. R. Percudani, A. Peracchi, The B6 database: a tool for the description and classification of
621 vitamin B6-dependent enzymatic activities and of the corresponding protein families. *BMC*
622 *Bioinformatics* **10**, 273 (2009).
623 26. M. Parra, S. Stahl, H. Hellmann, Vitamin B(6) and Its Role in Cell Metabolism and Physiology.
624 *Cells* **7** (2018).
625 27. J. Ciapaite *et al.*, Maintenance of cellular vitamin B(6) levels and mitochondrial oxidative
626 function depend on pyridoxal 5'-phosphate homeostasis protein (PLPHP). *J Biol Chem*
627 10.1016/j.jbc.2023.105047, 105047 (2023).
628 28. A. Fux, S. A. Sieber, Biochemical and Proteomic Studies of Human Pyridoxal 5'-Phosphate-
629 Binding Protein (PLPBP). *ACS Chem Biol* **15**, 254-261 (2020).
630 29. Y. M. Jang *et al.*, Human pyridoxal phosphatase. Molecular cloning, functional expression,
631 and tissue distribution. *J Biol Chem* **278**, 50040-50046 (2003).
632 30. E. Jeanclos *et al.*, Improved cognition, mild anxiety-like behavior and decreased motor
633 performance in pyridoxal phosphatase-deficient mice. *Biochim Biophys Acta Mol Basis Dis*
634 **1865**, 193-205 (2019).
635 31. C. Liu, C. B. Chan, K. Ye, 7,8-dihydroxyflavone, a small molecular TrkB agonist, is useful for
636 treating various BDNF-implicated human disorders. *Transl Neurodegener* **5**, 2 (2016).
637 32. C. S. Wang, E. T. Kavalali, L. M. Monteggia, BDNF signaling in context: From synaptic
638 regulation to psychiatric disorders. *Cell* **185**, 62-76 (2022).
639 33. U. Boltaev *et al.*, Multiplex quantitative assays indicate a need for reevaluating reported
640 small-molecule TrkB agonists. *Sci Signal* **10** (2017).
641 34. P. Pankiewicz *et al.*, Do Small Molecules Activate the TrkB Receptor in the Same Manner as
642 BDNF? Limitations of Published TrkB Low Molecular Agonists and Screening for Novel TrkB
643 Orthosteric Agonists. *Pharmaceuticals (Basel)* **14** (2021).
644 35. D. Todd *et al.*, A monoclonal antibody TrkB receptor agonist as a potential therapeutic for
645 Huntington's disease. *PLoS One* **9**, e87923 (2014).
646 36. J. Chen *et al.*, Antioxidant activity of 7,8-dihydroxyflavone provides neuroprotection against
647 glutamate-induced toxicity. *Neurosci Lett* **499**, 181-185 (2011).
648 37. M. L. Fonda, D. K. Eggers, S. Auerbach, L. Fritsch, Vitamin B-6 metabolism in the brains of
649 young adult and senescent mice. *Exp Gerontol* **15**, 473-479 (1980).
650 38. A. Gohla, Do metabolic HAD phosphatases moonlight as protein phosphatases? *Biochim*
651 *Biophys Acta Mol Cell Res* **1866**, 153-166 (2019).
652 39. A. Seifried *et al.*, Evolutionary and structural analyses of mammalian haloacid dehalogenase-
653 type phosphatases AUM and chronophin provide insight into the basis of their different
654 substrate specificities. *J Biol Chem* **289**, 3416-3431 (2014).
655 40. E. Jeanclos *et al.*, Glycolytic flux control by drugging phosphoglycolate phosphatase. *Nat*
656 *Commun* **13**, 6845 (2022).
657 41. M. Congreve, R. Carr, C. Murray, H. Jhoti, A 'rule of three' for fragment-based lead discovery?
658 *Drug Discov Today* **8**, 876-877 (2003).
659 42. J. O'Connell *et al.*, Small molecules that inhibit TNF signalling by stabilising an asymmetric
660 form of the trimer. *Nat Commun* **10**, 5795 (2019).
661 43. A. Seifried, J. Schultz, A. Gohla, Human HAD phosphatases: structure, mechanism, and roles
662 in health and disease. *Febs j* **280**, 549-571 (2013).
663 44. A. M. Burroughs, K. N. Allen, D. Dunaway-Mariano, L. Aravind, Evolutionary genomics of the
664 HAD superfamily: understanding the structural adaptations and catalytic diversity in a
665 superfamily of phosphoesterases and allied enzymes. *J Mol Biol* **361**, 1003-1034 (2006).
666 45. H. Huang *et al.*, Panoramic view of a superfamily of phosphatases through substrate
667 profiling. *Proc Natl Acad Sci U S A* **112**, E1974-1983 (2015).
668 46. C. Kestler *et al.*, Chronophin dimerization is required for proper positioning of its substrate
669 specificity loop. *J Biol Chem* **289**, 3094-3103 (2014).

670 47. K. N. Allen, D. Dunaway-Mariano, Phosphoryl group transfer: evolution of a catalytic scaffold.
671 *Trends Biochem Sci* **29**, 495-503 (2004).
672 48. G. Knobloch *et al.*, Synthesis of hydrolysis-resistant pyridoxal 5'-phosphate analogs and their
673 biochemical and X-ray crystallographic characterization with the pyridoxal phosphatase
674 chronophin. *Bioorg Med Chem* **23**, 2819-2827 (2015).
675 49. Z. Zhang *et al.*, 7,8-dihydroxyflavone prevents synaptic loss and memory deficits in a mouse
676 model of Alzheimer's disease. *Neuropsychopharmacology* **39**, 638-650 (2014).
677 50. L. Devi, M. Ohno, 7,8-dihydroxyflavone, a small-molecule TrkB agonist, reverses memory
678 deficits and BACE1 elevation in a mouse model of Alzheimer's disease.
679 *Neuropsychopharmacology* **37**, 434-444 (2012).
680 51. E. Bollen *et al.*, 7,8-Dihydroxyflavone improves memory consolidation processes in rats and
681 mice. *Behav Brain Res* **257**, 8-12 (2013).
682 52. N. A. Castello *et al.*, 7,8-Dihydroxyflavone, a small molecule TrkB agonist, improves spatial
683 memory and increases thin spine density in a mouse model of Alzheimer disease-like
684 neuronal loss. *PLoS One* **9**, e91453 (2014).
685 53. N. Aytan *et al.*, Protective effects of 7,8-dihydroxyflavone on neuropathological and
686 neurochemical changes in a mouse model of Alzheimer's disease. *Eur J Pharmacol* **828**, 9-17
687 (2018).
688 54. L. Gao *et al.*, TrkB activation by 7, 8-dihydroxyflavone increases synapse AMPA subunits and
689 ameliorates spatial memory deficits in a mouse model of Alzheimer's disease. *J Neurochem*
690 **136**, 620-636 (2016).
691 55. A. Akhtar, J. Dhaliwal, S. P. Sah, 7,8-Dihydroxyflavone improves cognitive functions in ICV-STZ
692 rat model of sporadic Alzheimer's disease by reversing oxidative stress, mitochondrial
693 dysfunction, and insulin resistance. *Psychopharmacology (Berl)* **238**, 1991-2009 (2021).
694 56. Y. H. Hsiao, H. C. Hung, S. H. Chen, P. W. Gean, Social interaction rescues memory deficit in
695 an animal model of Alzheimer's disease by increasing BDNF-dependent hippocampal
696 neurogenesis. *J Neurosci* **34**, 16207-16219 (2014).
697 57. A. Blugeot *et al.*, Vulnerability to depression: from brain neuroplasticity to identification of
698 biomarkers. *J Neurosci* **31**, 12889-12899 (2011).
699 58. J. C. Zhang *et al.*, Antidepressant effects of TrkB ligands on depression-like behavior and
700 dendritic changes in mice after inflammation. *Int J Neuropsychopharmacol* **18** (2014).
701 59. W. Yao *et al.*, Role of Keap1-Nrf2 signaling in depression and dietary intake of glucoraphanin
702 confers stress resilience in mice. *Sci Rep* **6**, 30659 (2016).
703 60. M. W. Zhang, S. F. Zhang, Z. H. Li, F. Han, 7,8-Dihydroxyflavone reverses the depressive
704 symptoms in mouse chronic mild stress. *Neurosci Lett* **635**, 33-38 (2016).
705 61. Y. Li *et al.*, Inflammation-activated C/EBPbeta mediates high-fat diet-induced depression-like
706 behaviors in mice. *Front Mol Neurosci* **15**, 1068164 (2022).
707 62. N. Amin *et al.*, Optimized integration of fluoxetine and 7, 8-dihydroxyflavone as an efficient
708 therapy for reversing depressive-like behavior in mice during the perimenopausal period.
709 *Prog Neuropsychopharmacol Biol Psychiatry* **101**, 109939 (2020).
710 63. E. J. Jaehne *et al.*, TrkB agonist 7,8-dihydroxyflavone reverses an induced prepulse inhibition
711 deficit selectively in maternal immune activation offspring: implications for schizophrenia.
712 *Behav Pharmacol* **32**, 404-412 (2021).
713 64. M. Han *et al.*, Intake of 7,8-Dihydroxyflavone During Juvenile and Adolescent Stages Prevents
714 Onset of Psychosis in Adult Offspring After Maternal Immune Activation. *Sci Rep* **6**, 36087
715 (2016).
716 65. Y. J. Yang *et al.*, Small-molecule TrkB agonist 7,8-dihydroxyflavone reverses cognitive and
717 synaptic plasticity deficits in a rat model of schizophrenia. *Pharmacol Biochem Behav* **122**,
718 30-36 (2014).
719 66. M. Han, J. C. Zhang, K. Hashimoto, Increased Levels of C1q in the Prefrontal Cortex of Adult
720 Offspring after Maternal Immune Activation: Prevention by 7,8-Dihydroxyflavone. *Clin*
721 *Psychopharmacol Neurosci* **15**, 64-67 (2017).

722 67. Q. Ren *et al.*, Effects of TrkB agonist 7,8-dihydroxyflavone on sensory gating deficits in mice
723 after administration of methamphetamine. *Pharmacol Biochem Behav* **106**, 124-127 (2013).
724 68. C. Becker *et al.*, Predicting and treating stress-induced vulnerability to epilepsy and
725 depression. *Ann Neurol* **78**, 128-136 (2015).
726 69. A. Guarino *et al.*, Low-dose 7,8-Dihydroxyflavone Administration After Status Epilepticus
727 Prevents Epilepsy Development. *Neurotherapeutics* **19**, 1951-1965 (2022).
728 70. R. A. Johnson *et al.*, 7,8-dihydroxyflavone exhibits therapeutic efficacy in a mouse model of
729 Rett syndrome. *J Appl Physiol (1985)* **112**, 704-710 (2012).
730 71. M. S. Kang *et al.*, Autism-like behavior caused by deletion of vaccinia-related kinase 3 is
731 improved by TrkB stimulation. *J Exp Med* **214**, 2947-2966 (2017).
732 72. Y. Lee, P. L. Han, Early-Life Stress in D2 Heterozygous Mice Promotes Autistic-like Behaviors
733 through the Downregulation of the BDNF-TrkB Pathway in the Dorsal Striatum. *Exp Neurobiol*
734 **28**, 337-351 (2019).
735 73. Y. S. Chen *et al.*, Early 7,8-Dihydroxyflavone Administration Ameliorates Synaptic and
736 Behavioral Deficits in the Young FXS Animal Model by Acting on BDNF-TrkB Pathway. *Mol*
737 *Neurobiol* **60**, 2539-2552 (2023).
738 74. M. Majewski, A. Kozlowska, M. Thoene, E. Lepiarczyk, W. J. Grzegorzewski, Overview of the
739 role of vitamins and minerals on the kynurenine pathway in health and disease. *J Physiol*
740 *Pharmacol* **67**, 3-19 (2016).
741 75. M. A. Sorolla *et al.*, Impaired PLP-dependent metabolism in brain samples from Huntington
742 disease patients and transgenic R6/1 mice. *Metab Brain Dis* **31**, 579-586 (2016).
743 76. S. W. Jang *et al.*, A selective TrkB agonist with potent neurotrophic activities by 7,8-
744 dihydroxyflavone. *Proc Natl Acad Sci U S A* **107**, 2687-2692 (2010).
745 77. K. Kobayashi, H. Suzuki, Synapse-selective rapid potentiation of hippocampal synaptic
746 transmission by 7,8-dihydroxyflavone. *Neuropsychopharmacol Rep* **38**, 197-203 (2018).
747 78. D. Talwar *et al.*, Optimisation and validation of a sensitive high-performance liquid
748 chromatography assay for routine measurement of pyridoxal 5-phosphate in human plasma
749 and red cells using pre-column semicarbazide derivatisation. *Journal of chromatography. B,*
750 *Analytical technologies in the biomedical and life sciences* **792**, 333-343 (2003).
751 79. C. A. Wartchow *et al.*, Biosensor-based small molecule fragment screening with biolayer
752 interferometry. *J Comput Aided Mol Des* **25**, 669-676 (2011).
753 80. A. J. McCoy *et al.*, Phaser crystallographic software. *J Appl Crystallogr* **40**, 658-674 (2007).

754

755

FIGURES AND FIGURE LEGENDS

Figure 1. Role of PDXP in hippocampal PLP homeostasis.

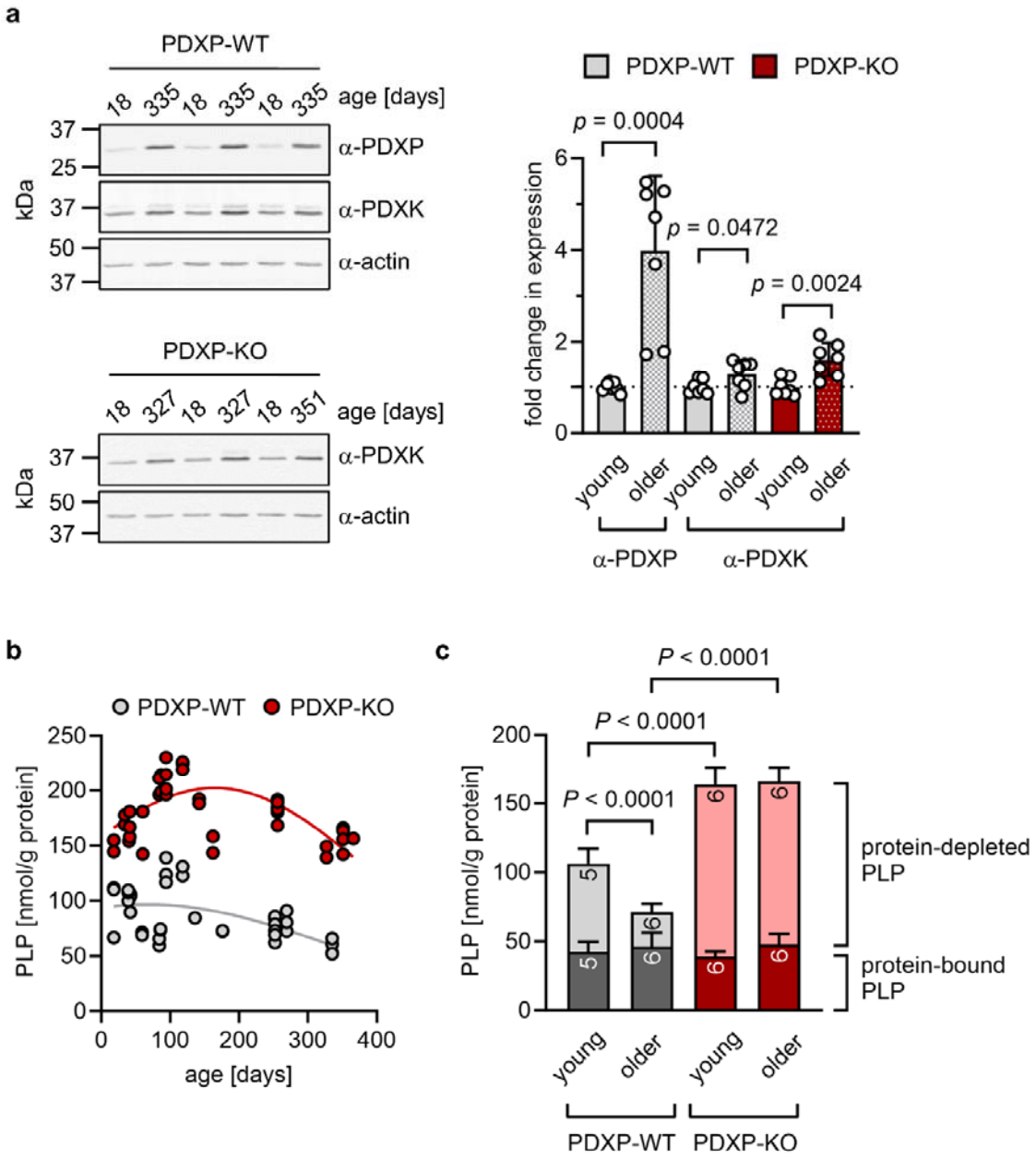

(**a**) Age-dependent expression of PDXK and PDXP in murine hippocampi. *Left panels*, representative Western blots of three hippocampi for each genotype. The same blots were reprobed with α-actin antibodies as a loading control. The age of the investigated mice is indicated above the blots. *Right panel*, densitometric quantification of hippocampal PDXP

763 and PDXK Western blot signals, corrected by the corresponding actin signals. Young mice
764 were 18-42 days old, older mice were 252-351 days old; *n*=7 hippocampi were analyzed per
765 group. Data are mean values ± S.D. Statistical analysis was performed with unpaired, two-
766 sided *t*-tests; *p*-values are indicated. (**b**) Age-dependent, total PLP-concentrations in isolated
767 hippocampi of PDXP-WT and PDXP-KO mice. PLP was derivatized with semicarbazide and
768 analyzed by HPLC. Each symbol represents the result of the PLP determination in an
769 individual hippocampus. Data were fitted by Gaussian least-squares analyses. (**c**)
770 Determination of protein-bound and protein-depleted PLP in PDXP-WT and PDXP-KO
771 hippocampal lysates of young (18-42 days old) and older mice (252-352 days old). The
772 number of analyzed hippocampi is indicated in the bars. Data are mean values ± S.D.
773 Statistical analysis was performed with two-way ANOVA and Tukey's multiple comparisons
774 test. Significant differences (adjusted *P*-values) in protein-depleted PLP levels are indicated.
775 The exact age of analyzed mice is listed in **Figure 1 – supplementary figure 1**. **Source data**
776 are available for this Figure.

777 **Figure 2: Characterization of the 7,8-DHF/PDXP interaction.**

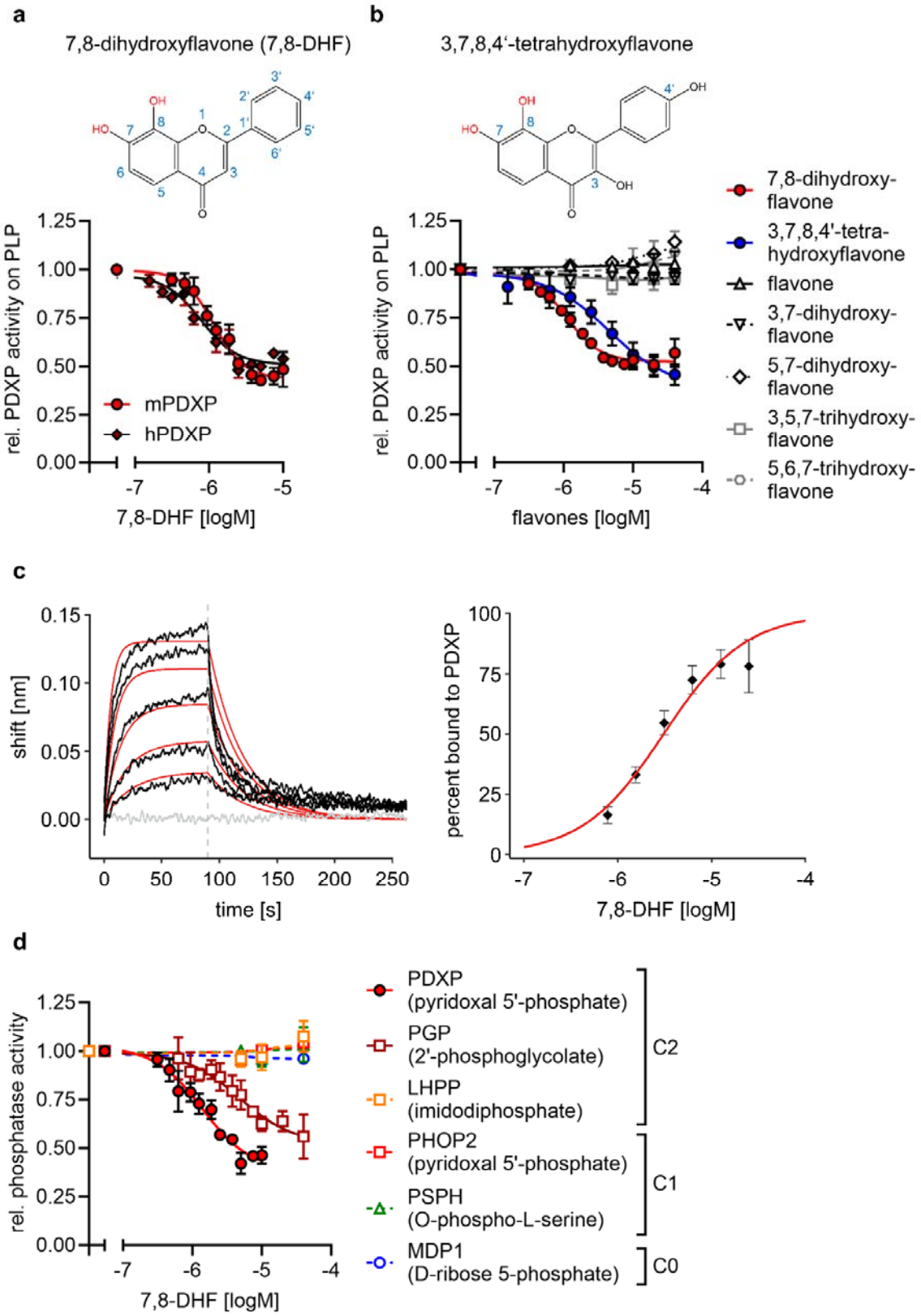

778

(**a**) Determination of half-maximal inhibitory constants (IC_{50}) of 7,8-DHF (2D-structure shown on top) for purified murine or human PDXP, using pyridoxal 5'-phosphate (PLP) as a substrate. Phosphatase activities in the presence of 7,8-DHF were normalized to the respective enzyme activities measured in the presence of the DMSO solvent control. Data are mean values ± S.D. of *n*=3 (human PDXP) and *n*=4 (murine PDXP) independent experiments. (**b**) IC_{50} values of different flavones for purified murine PDXP with PLP as a substrate. Phosphatase activities in the presence of flavones were normalized to the respective enzyme activities in the presence of the DMSO solvent control. All data are mean values ± S.D. The inhibition of PDXP by 3,7,8-trihydroxyflavone-4'-hydroxyphenyl (2D-structure shown on top) was assessed in *n*=6 independent experiments. All other data are from *n*=3 biologically independent experiments. Apparently missing error bars are hidden by the symbols. (**c**) Biolayer interferometry (BLI) measurements of the interaction of 7,8-DHF with purified murine PDXP. *Left panel*, example sensorgram overlayed with the global 1:1 binding model (red) and the negative control (gray). The dashed line indicates the start of the dissociation phase. *Right panel*, steady-state dose-response analysis for 7,8-DHF based on *n*=4 measurements. (**d**) Sensitivity of the indicated HAD phosphatases to 7,8-DHF. Phosphatase activities in the presence of 7,8-DHF were normalized to the respective enzyme activities measured in the presence of the DMSO solvent control. Data are mean values ± S.D. of *n*=4 (PGP) or *n*=3 independent experiments (all other phosphatases). Phosphatase substrates and cap types are indicated in the legend. PGP, phosphoglycolate phosphatase; LHPP, phospholysine phosphohistidine inorganic pyrophosphate phosphatase; PHOP2, phosphatase orphan 2; PSPH, phosphoserine phosphatase; MDP1, magnesium-dependent phosphatase-1. **Source data** are available for this Figure.

803 **Figure 3. X-ray crystal structure of murine PDXP in complex with 7,8-DHF.**

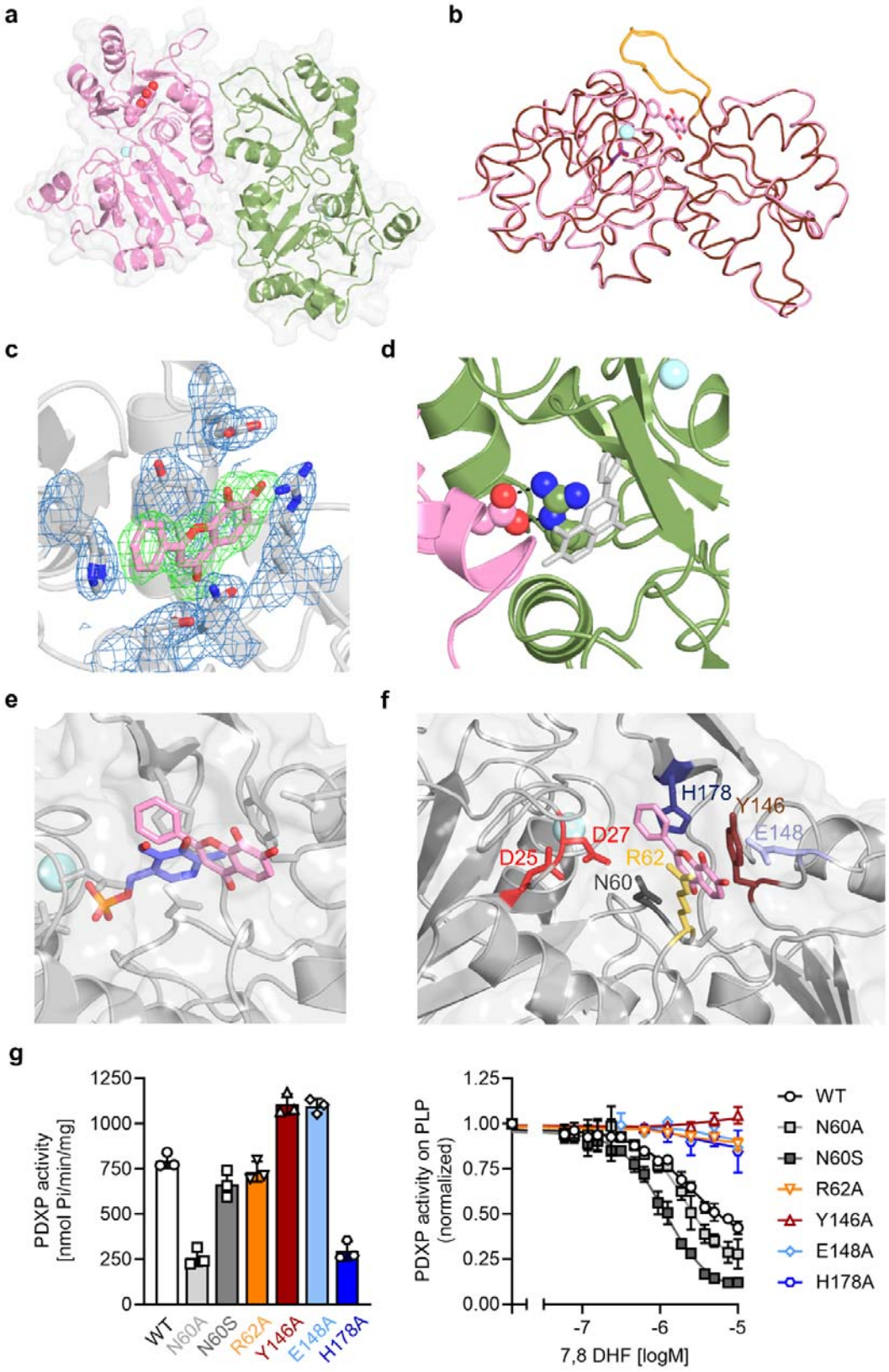

804

(**a**) The model was refined to a resolution of 2.0 Å (PDB code 8QFW). Protomer A of full-length, homodimeric PDXP is shown in pink and protomer B in green. 7,8-DHF is shown in sphere representation with its C-atoms in pink and the catalytically essential Mg^{2+} ions are shown as cyan spheres. (**b**) Structural overlay of apo-PDXP (PDB code 4BX3, chain A, in brown) and the 7,8-DHF-bound PDXP protomer A (in pink). 7,8-DHF is shown in stick representation with its C-atoms in pink. The catalytic Asp25 residues are shown in red or purple sticks, respectively, and the Mg^{2+} ion is depicted as a cyan sphere. The substrate specificity loops are highlighted in yellow. (**c**) $2F_o$-F_c electron density map contoured at an RMSD of 1 in blue, overlaid with the refined model. The F_o-F_c map of 7,8-DHF contoured at an RMSD of 3 is shown with positive densities in green mesh. (**d**) Arg62 blocks 7,8-DHF binding in the B-protomer. A salt bridge between Arg62 (C-atoms shown as green spheres) in the B-protomer (in green) and Asp14 (C-atoms shown as pink spheres) of a symmetry-related A-protomer (in pink) blocks the 7,8-DHF binding site. 7,8-DHF (in stick representation with gray C-atoms) is modeled based on the A-protomer. (**e**) Comparison of the 7,8-DHF and PLP binding sites. The active site of 7,8-DHF-bound PDXP is in gray. 7,8-DHF is shown in stick representation (pink C-atoms), and the Mg^{2+} ion as a cyan sphere. PLP (in stick representation with blue C-atoms) was modelled based on a superposition of the human PDXP-PLP complex (PDB code 2CFT). (**f**) Structural details of bound 7,8-DHF and adjacent residues of the active site. (**g**) Verification of 7,8-DHF - PDXP interactions. *Left panel*, phosphatase activity of purified PDXP or the indicated PDXP variants. Data are mean values ± S.D. of n=3 independent experiments. *Right panel*, determination of the IC_{50} values of 7,8-DHF for purified PDXP or the indicated PDXP variants. Data are mean values ± S.D. of n=3 independent experiments. Apparently missing error bars are hidden by the symbols. **Source data** are available for this Figure.

831 **Figure 4. Effect of 7,8-DHF on the PLP/PL ratio in cultured hippocampal neurons from**

832 **WT or PDXP-KO mice**.

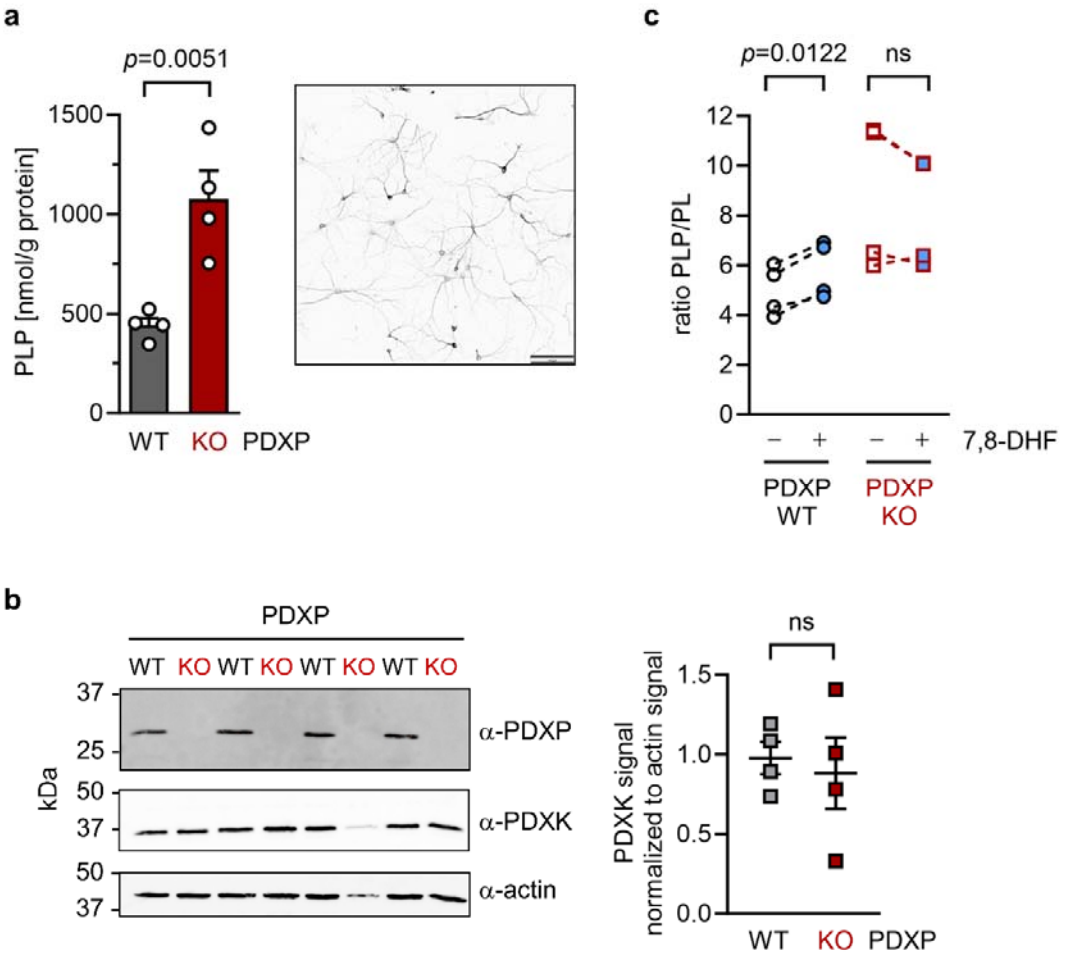

833

834 (**a**) Effect of long-term PDXP deficiency on total PLP levels in hippocampal neurons. Data

835 are mean values ± S.E. of *n*=4 independent experiments. Statistical significance was assessed

836 with a two-tailed, unpaired *t*-test. A representative image of primary hippocampal neurons

837 stained for the neuronal marker protein MAP2 is shown in the insert (pixel intensities were

838 color-inverted for better visualization). Scale bar, 100 µm. (**b**) Western blot analysis of PDXP

839 and PDXK expression in hippocampal neuron samples shown in (a). The same blots were

840 reprobed with α-actin antibodies as a loading control. The densitometric quantification of

841 PDXK signals is shown on the right; data are mean values ± S.E. of *n*=4 independent

842 experiments. (**c**) Effect of 7,8-DHF (20 µM, 45 min) or the DMSO solvent control (0.02%

843 v/v, 45 min) on the PLP/PL ratio in hippocampal neurons of PDXP-WT or PDXP-KO mice.

844 **Source data** are available for this Figure.

845 **TABLES**

846

847 **Table 1. Kinetic constants of PDXP-catalyzed PLP hydrolysis in the presence of 7,8-**

848 **DHF.**

849

7,8-DHF [μM]	0	1.0	1.5	2.0	3.0	5.0	10.0
K_M [μM]	14.98 ± 1.28	18.54 ± 6.24	20.20 ± 6.19	18.97 ± 5.15	24.83 ± 2.61	32.96 ± 2.13	30.61 ± 2.57
v_{max} [μmol/min/mg]	1.08 ± 0.04	0.95 ± 0.01	0.89 ± 0.04	0.85 ± 0.02	0.80 ± 0.04	0.81 ± 0.05	0.74 ± 0.06
k_{cat} [s^{-1}]	0.57 ± 0.02	0.5 ± 0.01	0.47 ± 0.02	0.45 ± 0.01	0.42 ± 0.02	0.43 ± 0.03	0.39 ± 0.03
k_{cat}/K_M [$s^{-1}\cdot M^{-1}$] ($\times 10^{-4}$)	3.93 ± 0.29	3.27 ±0.84	2.75 ± 0.67	2.72 ± 0.66	1.72 ±0.10	1.31 ± 0.06	1.29 ± 0.01

850

851 The data are mean values ± S.E.M. of *n*=3 independent experiments, except for the solvent
852 control samples (*n*=6). Curves were fitted and parameters K_M (Michaelis–Menten constant);
853 v_{max}, (maximum enzyme velocity); k_{cat} (turnover number) were derived using the Michaelis-
854 Menten model in GraphPad Prism 9.5.1. The k_{cat} values were calculated from the maximum
855 enzyme velocities using a molecular mass of 31,828 Da for PDXP. DMSO concentrations
856 were kept constant (0.1% DMSO under all conditions, including the solvent control samples).

857

858

Table 2. Data Collection and Refinement Statistics.

	PDXP-7,8-DHF
Data collection	
Space group	I23
a, *b*, *c* (Å)	167.01, 167.01, 167.01
α, β, γ (°)	90, 90, 90
Resolution (Å)	47.21 - 2.00 (2.07-2.00)
[a]R_{sym}	0.190 (4.101)
[b]R_{pim}	0.030 (0.652)
$CC_{1/2}$	1.00 (0.459)
[c]$<I/\sigma I>$	20.67 (1.06)
Completeness	0.998 (0.973)
Redundancy	41.0 (38.5)
Refinement	
Resolution (Å)	20.00 – 2.00 (2.07-2.00)
[d]R-work	0.1838 (0.300)
[e]R-free	0.21 (0.322)
RMS deviations in	
Bond lengths (Å)	0.002
Bond angles (°)	0.50
Chiral centers ($Å^3$)	0.038
Planar groups (Å)	0.005
Estimated coordinate error (Å)	0.26
Ramachandran statistics (%)	98.95/1.05/0

[a]$R_{sym} = \Sigma_{hkl}\Sigma_i \mid I_i - <I> \mid / \Sigma_{hkl}\Sigma_i I_i$ where I_i is the ith measurement and $<I>$ is the weighted mean of all measurements of I.

[b]$R_{pim} = \Sigma_{hkl} 1/(N-1)^{½} \Sigma_i \mid I_i(hkl) - \overline{I(hkl)} \mid / \Sigma_{hkl}\Sigma_i I(hkl)$, where N is the redundancy of the data and $\overline{I(hkl)}$ the average intensity.

[c]$<I/\sigma I>$ indicates the average of the intensity divided by its standard deviation.

[d]$R_{work} = \Sigma_{hkl} \mid\mid F_o\mid - \mid F_c\mid\mid / \Sigma_{hkl}\mid F_o\mid$ where F_o and F_c are the observed and calculated structure factor amplitudes.

[e]R_{free} same as R for 5% of the data randomly omitted from the refinement. The number of reflections includes the R_{free} subset.

Numbers in parentheses refer to the highest resolution data shell.

Ramachandran statistics reflect the percentage of residues in favored/allowed/outlier regions.

873 **SUPPLEMENTARY INFORMATION**

874

875 **Figure 1 – figure supplement 1. Analysis of total hippocampal PLP levels in PDXP-WT**
876 **and PDXP-KO mice.**

877

PDXP-WT		PDXP-KO	
age [days]	PLP [nmol/g protein]	age [days]	PLP [nmol/g protein]
18	66.77	18	**154.60**
18	**111.66**	18	**144.50**
18	**110.11**	18	**154.74**
39	**99.73**	34	**169.06**
39	107.59	34	**177.57**
39	109.60	40	153.93
42	89.62	41	**180.65**
42	**105.82**	41	157.84
42	**104.38**	41	166.67
59	71.55	60	180.58
59	68.99	60	142.33
84	59.36	87	214.52
84	65.52	87	198.61
86	73.50	94	196.21
86	74.40	94	211.20
94	123.81	94	214.70
94	116.81	94	201.21
94	138.95	94	230.42
136	84.61	142	192.13
176	72.22	142	188.03
176	72.83	162	143.41
252	**83.47**	162	158.23
252	**85.78**	256	**180.26**
252	**78.88**	256	**184.36**
252	72.86	256	**168.17**
252	62.20	256	191.69
252	69.15	256	182.87
269	72.53	256	189.11
269	90.90	327	149.04
269	80.60	327	139.20
335	52.90	351	165.84
335	**60.93**	351	**163.33**
335	**52.17**	351	**142.23**
335	**65.93**	351	**155.71**
		366	156.26

878

879 Each value represents the result of the PLP determination in an individual hippocampus.
880 Analysis for a statistically significant difference between PLP levels in PDXP-WT and

881 PDXP-KO hippocampi (all ages combined; two-tailed, unpaired *t*-test) $p<0.0001$. Bold table
882 entries indicate those hippocampal extracts that were further separated for an analysis of
883 protein-depleted and protein-bound PLP (see **Fig. 1c**).
884
885

886 **Figure 2 – figure supplement 1. Identification of PDXP inhibitors.**

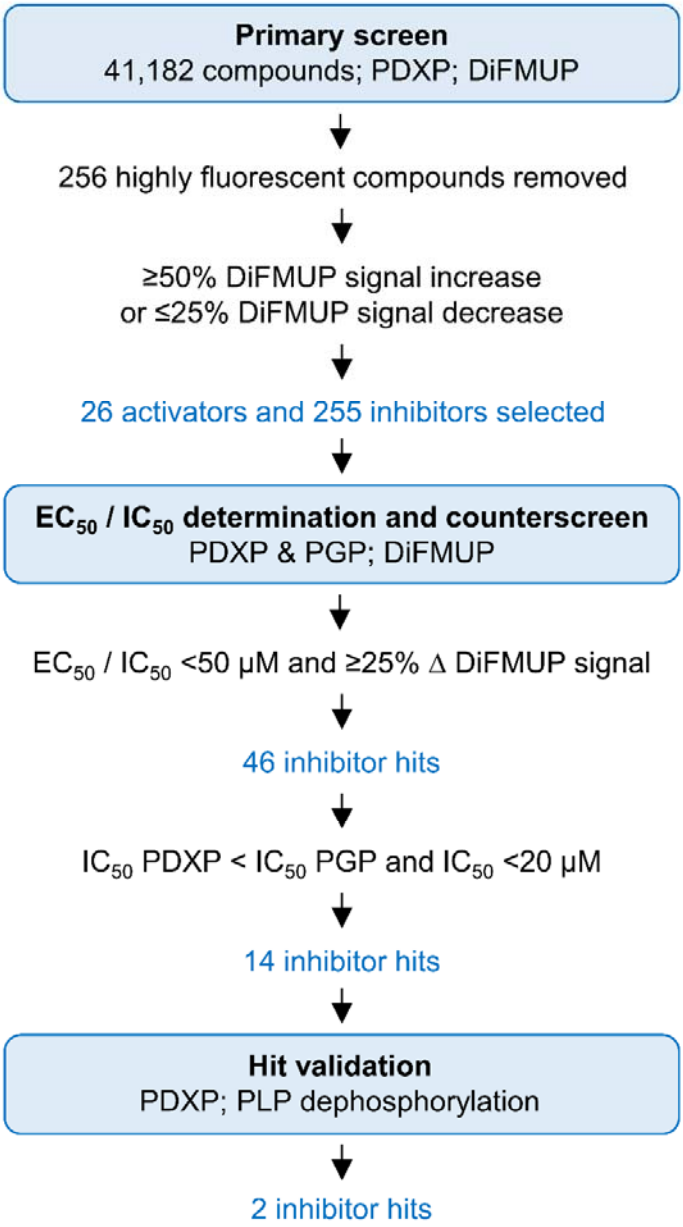

887

888 A primary screen was conducted using 6,8-difluoro-4-methylumbelliferyl phosphate
889 (DiFMUP) as an artificial substrate. Out of 41,182 screened compounds, 256 compounds
890 were discarded that showed very high autofluorescence (as recognized by elevated
891 fluorescence at the start of the kinetic curve); 26 compounds showed statistically significant
892 PDXP activation, and 255 compounds showed PDXP inhibition (as recognized by an elevated
893 or decreased slope of the kinetic curve, respectively). The average Z'-factor of the screen was
894 0.75 ± 0.112. These 281 compounds were selected for DiFMUP-based concentration-
895 dependent validation, and the 46 most potent compounds were selected. A counter-screening

896 was conducted in parallel, also in a concentration-dependent fashion, against the PDXP
897 paralog and closest relative phosphoglycolate phosphatase (PGP). The 14 compounds that
898 were inactive against PGP were validated in a secondary assay, using the PDXP substrate
899 pyridoxal 5'-phosphate (PLP). Two PDXP inhibitor hits blocked PLP dephosphorylation by
900 ≥50%. **Source data** are available for this Figure.
901
902

903 **Figure 2 – figure supplement 2. PDXP inhibitor hits.**

904

	InChI Key	IC_{50} [µM]
7,8-DHF	COCYGNDCWFKTMF-UHFFFAOYSA-N	0.8 *
	FMP-1	~1
	RDMYXZLESVAHOO-UHFFFAOYSA-N	>40
	FMP-2	>40
	RBZAGLIUHTVMFL-UHFFFAOYSA-N	>40
	FMP-3	>40
	HSJXOMZEPTVVQC-UHFFFAOYSA-N	>40
	PRAORRBPQXAGQD-UHFFFAOYSA-N	>40
	BMXOLQCTPIQVOD-UHFFFAOYSA-N	>40
	GYJACFGQPFXKCA-UHFFFAOYSA-N	>40
	PCRFOVGMSDFVLC-UHFFFAOYSA-N	>40
	FHXDSQYFCFWKAW-UHFFFAOYSA-N	>40
	OPTDAYWBFJRIGB-UHFFFAOYSA-N	>40
	GCUCIFQCGJIRNT-UHFFFAOYSA-N	>40

905

906 Determination of half-maximal inhibitory constants (IC_{50}) of 14 PDXP inhibitory compounds
907 (see InChI Key for chemical substance identification) using purified murine PDXP and
908 pyridoxal 5'-phosphate (PLP) as a substrate. Data marked with an asterisk (*) are results of
909 *n*=3 independent experiments. Because of the limited quantity of most compounds available
910 for these assays, all other data are results of *n*=1 determinations. 7,8-DHF, 7,8-
911 dihydroxyflavone; ~, approximate IC_{50} value. FMP-1, FMP-2 and FMP-3 are compounds
912 obtained from academic donors whose structure is undisclosed for intellectual property
913 reasons.

914

915

916 **Figure 2 – figure supplement 3. BLI measurements of the interaction of 7,8-DHF with**
917 **purified murine PDXP.**
918

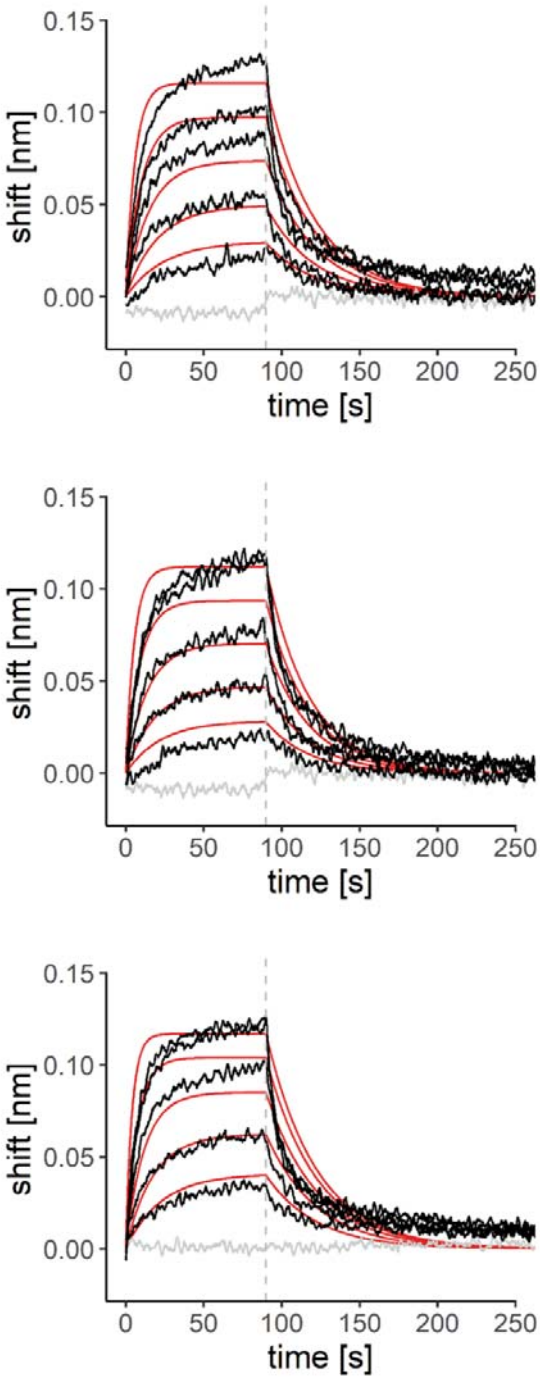

919
920 Sensorgrams of three additional experiments overlayed with the global 1:1 binding model
921 (red) and the negative control (gray). The dashed line indicates the start of the dissociation
922 phase.
923

924 **Figure 3 – figure supplement 1. Unit cell environment of the 7,8-DHF · PDXP crystal.**

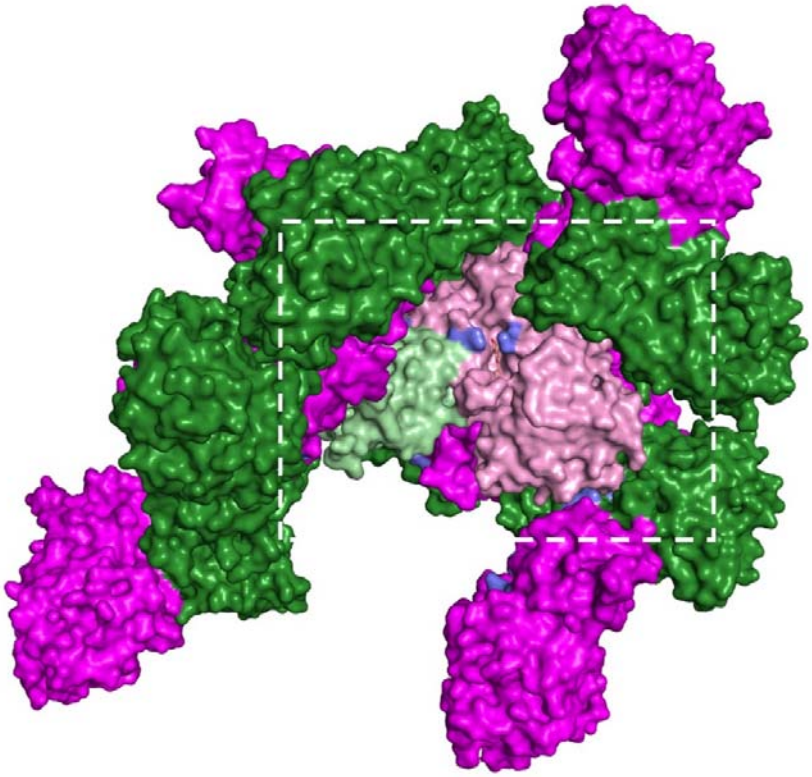

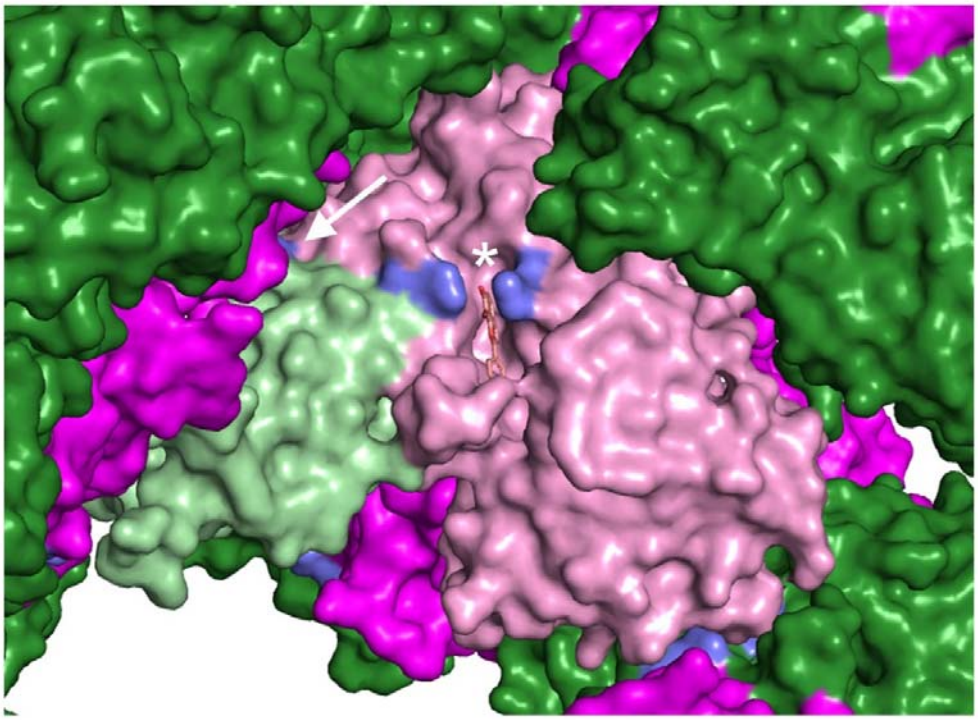

925

926

927 The 7,8-DHF-bound protomer A is depicted in pink, the inhibitor-free protomer B is colored
928 in light green. 7,8-DHF is shown in stick representation (C-atoms in pink), and its position is
929 marked with a white asterisk. Arg62 and Glu148 at the active site entrances of protomers A
930 and B are highlighted in blue. Surrounding symmetry mates within 4 Å of the centrally
931 located 7,8-DHF-PDXP/apo-PDXP dimer are shown in surface representation in magenta or
932 dark green. Whereas the active site in 7,8-DHF-bound protomer A is accessible, the
933 corresponding site in protomer B is shielded by two crystallographic neighbors (white arrow).
934 The marked area is enlarged in the bottom panel. **Source data** are available for this Figure.
935
936

Figure 3 – figure supplement 2. Alignment of human and murine PDXP.

```
PDXP_HUMAN      MARCERLRGAALRDVLGRAQGVLFDCDGVLWNGERAVPGAPELLERLARAGKAALFVSNN 60
PDXP_MOUSE      MARCERLRGAALRDVLGQAQGVLFDCDGVLWNGERIVPGAPELLQRLARAGKNTLFVSNN 60
                *****************:***************** ********:******* :******

PDXP_HUMAN      SRRARPELALRFARLGFGGLRAEQLFSSALCAARLLRQRLPGPPDAPGAVFVLGGEGLRA 120
PDXP_MOUSE      SRRARPELALRFARLGFAGLRAEQLFSSALCAARLLRQRLSGPPDASGAVFVLGGEGLRA 120
                *****************.********************** ***** *************

PDXP_HUMAN      ELRAAGLRLAGDPSAGDGAAPRVRAVLVGYDEHFSFAKLREACAHLRDPECLLVATDRDP 180
PDXP_MOUSE      ELRAAGLRLAGDP----GEDPRVRAVLVGYDEQFSFSRLTEACAHLRDPDCLLVATDRDP 176
                *************    *  ************:***::* *********:**********

PDXP_HUMAN      WHPLSDGSRTPGTGSLAAAVETASGRQALVVGKPSPYMFECITENFSIDPARTLMVGDRL 240
PDXP_MOUSE      WHPLSDGSRTPGTGSLAAAVETASGRQALVVGKPSPYMFQCITEDFSVDPARTLMVGDRL 236
                ****************************************:****:**:************

PDXP_HUMAN      ETDILFGHRCGMTTVLTLTGVSRLEEAQAYLAAGQHDLVPHYYVESIADLTEGLED    296
PDXP_MOUSE      ETDILFGHRCGMTTVLTLTGVSSLEEAQAYLTAGQRDLVPHYYVESIADLMEGLED    292
                ********************** ********:***:************** *****
```

Protein sequences of human PDXP (UniProtKB Q96GD0) and murine PDXP (UniProtKB P60487) were aligned with the EMBL-EBI multiple sequence alignment tool Clustal Omega version 1.2.4. PDXP residues found to engage in 7,8-DHF interactions (highlighted in red color) are identical in human and murine PDXP.

Figure 3 – figure supplement 3. Purity of the employed PDXP and PDXP variants.

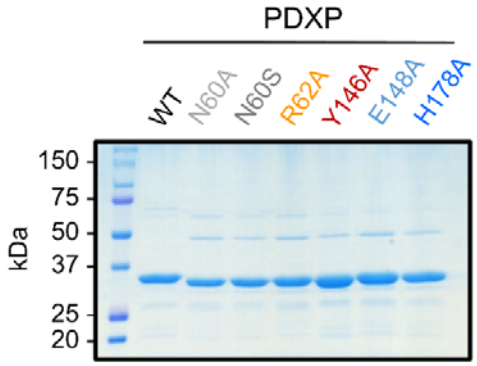

A Coomassie Blue-stained gel is shown.